Modeling of Hydrological Processes Using Unstructured and Irregular Grids: 2D Groundwater Application

J. Dehotin[1]; R. F. Vázquez[2]; I. Braud[3]; S. Debionne[4]; and P. Viallet[5]

Abstract: To better handle landscape heterogeneities in distributed hydrological modeling, an earlier work proposed a discretization based on nested levels, which leads to fully unstructured modeling meshes. Upon such a discretization, traditional numerical solutions must be adapted, especially to describe lateral flow between the unstructured mesh elements. In this paper, we illustrated the feasibility of the numeric solution of the diffusion equation, representing groundwater flow, using unstructured meshes. Thus, a two-dimensional (2D) groundwater model (BOUSS2D), adapted to convex unstructured and irregular meshes was developed. It is based on the approximation of the 2D Boussinesq equation using numeric techniques suitable for nonorthogonal grids. The handling of vertical and horizontal aquifer heterogeneities is also addressed. The fluxes through the interfaces among joined mesh elements are estimated by the finite volume method and the gradient approximation method. Comparisons between the BOUSS2D predictions and analytical solutions or predictions from existing codes suggest the acceptable performance of the BOUSS2D model. These results therefore encourage the further development of hydrological models using unstructured meshes that are capable of better representing the landscape heterogeneities.

DOI: 10.1061/(ASCE)HE.1943-5584.0000296

CE Database subject headings: Groundwater flow; Hydrologic models; Boussinesq equation; Heterogeneity; Grid systems.

Author keywords: Hydrological processes; Groundwater flow modeling; Boussinesq equation; Heterogeneity; Unstructured grid; Finite volume; Gradient approximation; Flux approximation.

Introduction

The growing concerns about environmental questions, climate change issues, as well as the emergence of the concept of sustainable development, have modified the requirements towards hydrological observation and modeling. Consideration of land-use and human-induced landscape modifications is now a major concern for water management problems (quantity and quality) such as flood forecasting, nonpoint source contamination, the study of the impact of land-use evolution on stream flow, pollutants, or sediments transport. Catchment heterogeneity is driven by topography, land use, geology, and pedology as well as human action (roads, urban areas, dams, etc.). Traditional grid squares are not well adapted to describe this heterogeneity. In this context, there is the need of developing integrated water cycle modeling approaches that include surface, subsurface, and groundwater processes, based on nonorthogonal and irregular computational meshes.

Hence, an alternative approach is the use of triangular irregular networks (TINs), constrained to follow hydrological limits such as the river network or saturated areas limits (Vivoni et al. 2004). The tRIBS hydrological model (Ivanov et al. 2004), built on such a discretization, allows the simulation of the whole water balance, but the number of computing units can be large (about 50,000 elements for a 1,000-km^2 catchment). Recently, Dehotin and Braud (2008) proposed a general methodology for catchment discretization allowing to take into account catchment heterogeneity according to the problem beforehand and the available data. It is based on nested discretization levels. The first level is defined by the river network and the associated subcatchments. These units can be further discretized into "homogeneous" units in terms of hydrological functioning called hydrolandscape (second level). Finally, if required by the numerical solutions, these units can be further discretized to fulfill geometrical constraints (third level) leading to the final mesh used for the modeling. The procedure leads to very irregular elements for the description of the land surface and one mesh can have a variable number of neighbors. An illustration is shown in Fig. 1. In general the number of modeling units is smaller than when using TINs. The large number of elements is not a great problem when only vertical transfer within soils is considered. The representation of lateral transfer within soils can however become more problematic on irregular elements. It can be based on an explicit calculation of the flux between two elements, as a function of the hydraulic gradient. (e.g., Ivanov et al. 2004 on TINs). Branger et al. (2008) also used this methodology on a discretization based on Dehotin and Braud (2008) principles. The question that was addressed is the follow-

[1]Doctor, Cemagref, UR HHLY, 3bis Quai Chauveau, CP 220, 69336 Lyon Cédex 9, France (corresponding author). E-mail: judicael.dehotin@cemagref.fr

[2]Senior Researcher, Unidad de Suelos y Riegos (asociada al CSIC), Centro de Investigación y Tecnología Agroalimentaria de Aragón (CITA), Avda. Montañana 930, 50059, Zaragoza, Spain; presently, Dirección de Investigación, Universidad de Cuenca, Av. 12 de Abril S/N, Cuenca, Ecuador. E-mail: raulfvazquezz@yahoo.co.uk

[3]Senior Researcher, Cemagref, UR HHLY, 3bis Quai Chauveau, CP 220, 69336 Lyon Cédex 9, France. E-mail: isabelle.braud@cemagref.fr

[4]Engineer, HYDROWIDE, 1025 Rue de la Piscine 38600 Saint-Martin d'Hères, France.

[5]Engineer, HYDROWIDE, 1025 Rue de la Piscine 38600 Saint-Martin d'Hères, France.

Note. This manuscript was submitted on March 18, 2009; approved on July 13, 2010; published online on July 19, 2010. Discussion period open until July 1, 2011; separate discussions must be submitted for individual papers. This paper is part of the ***Journal of Hydrologic Engineering***, Vol. 16, No. 2, February 1, 2011. ©ASCE, ISSN 1084-0699/2011/2-108–125/$25.00.

J. Hydrol. Eng. 2011.16:108-125.

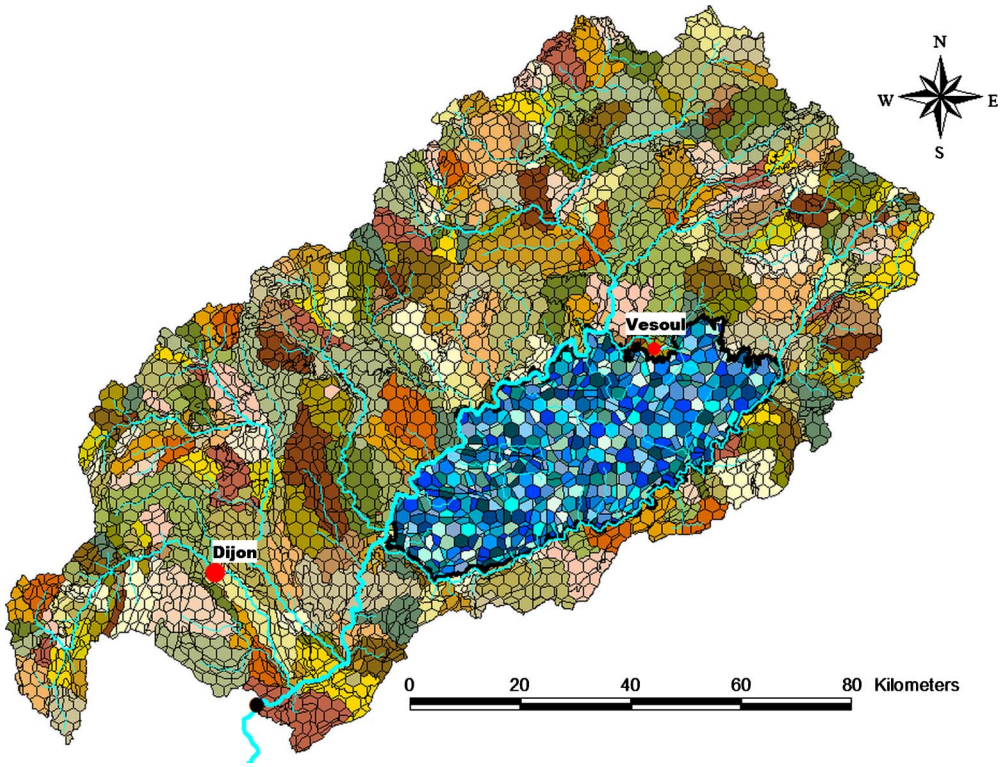

Fig. 1. Example of the irregular and unstructured mesh obtained after considering the soil surface description. The catchment (11,800 km^2) is the upper Saône located in France (Dehotin 2007).

ing: is it possible to solve traditional partial differential equations, describing water flow, on irregular elements, with efficient and stable numerical methods? The example of the diffusion equation representing groundwater flow in the saturated zone, of a heterogeneous porous media (both vertically and horizontally) was chosen to show the feasibility of the approach. The corresponding hydrological model, adapted to the study of the water balance on a catchment such as the one in Fig. 1 is the following. It is based on a one-dimensional vertical flow in the unsaturated zone, including the evapotranspiration process, coupled with a two-dimensional (2D) model in the saturated zone of the porous media. The model also include coupling between the river and the saturated zone. Vertical heterogeneity in the porous media is taken into account using horizontal discretization of soil profiles. For an easier coupling between the unsaturated and saturated zones the same irregular geometry for saturated and unsaturated zones was used. Thus in the following, we address the solution of the groundwater flow on an irregular geometry, where one cell can have various neighbors and the porous media can be heterogeneous both vertically and horizontally.

Many hydrological processes in porous media can be modeled using a diffusion equation. In this equation, the diffusion coefficient (or permeability) is a space dependent full tensor because of the heterogeneity of the porous media and the principal direction of this tensor is not necessarily aligned with the grids. Various numerical schemes on nonorthogonal meshes exist in the literature for the diffusion equation. Examples are the finite volumes methods (Cai 1990; Coudière et al. 1996; Eymard et al. 1997; Eymard et al. 1999; Jayantha and Turner 2003a,b); the multipoint flux approximations (Aavatsmark et al. 1994; Edwards 2002; Edwards and Rogers 1994, 1998; Verma and Aziz 1997; Aavatsmark 2002; Pal et al. 2006) or finite-element methods. Loudyi et al. (2007) developed a groundwater model based on a nonorthogonal quadrangular grid using the finite volume method and the improved least squared gradient reconstruction for the estimation of the water flux between elements. However, those results are still not used by the distributed hydrological modeling community, where unstructured meshes are in general based on TINs. In the following paragraphs, it is demonstrated that those techniques can efficiently be implemented for their use within integrated water cycle models. In this context, we present a new groundwater model called BOUSS2D that allows handling unstructured meshes with any number of neighboring cells, as well as subsoil heterogeneity and discontinuities. It is based on the resolution of the 2D Boussinesq equation (Anderson and Woessner 1992) on unstructured and irregular meshes, using the finite volumes method. The finite volumes technique was chosen because of its simplicity. Its advantages are twofold. It offers a great flexibility in geometrical shape handling and has the advantage of being unconditionally mass conservative (Barth and Ohlberger 2004). The fluxes between control volumes (CVs) are based on the approximation of the gradient along the CV faces. The implemented gradient approximation technique is based on the local gradient reconstruction.

Theoretical Background and Numerical Method

The finite volumes method technique is based on the integration of the governing equation over the CVs, independently of their shape. The flow variable can be associated to the vertex (cell vertex) or to a point inside the mesh (cell centered). In finite volumes methods, volume integrals of the governing equation are replaced by surface integrals using the Green's theorem. The numerical resolution of the governing equation corresponds to an

J. Hydrol. Eng. 2011.16:108-125.

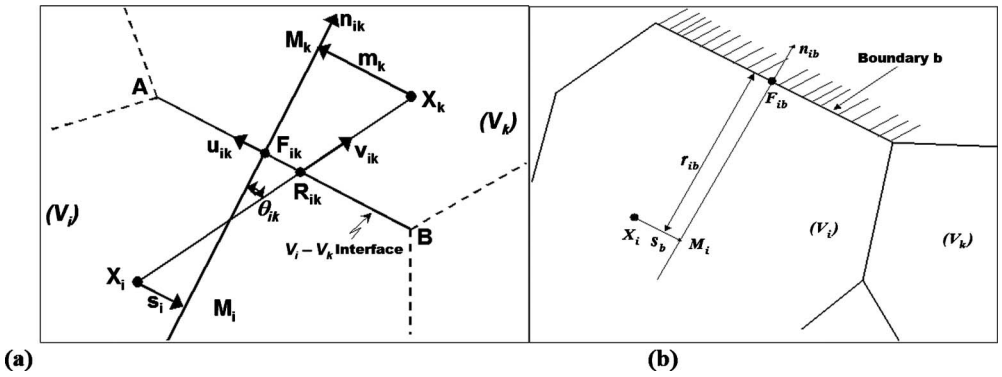

Fig. 2. Example of BOUSS2D mesh elements interface on (a) internal mesh elements; (b) boundary mesh elements

approximation of the flux between adjacent CVs. The groundwater flow in two dimensions is computed by the Boussinesq equation, which combines the continuity equation with the Darcy's law (Anderson and Woessner 1992).

Numeric Approximation of the Boussinesq Equation Using the Finite Volumes Method

The transient unconfined groundwater flow through porous media can be represented by the following Boussinesq equation in 2D (de Marsily 1981; Anderson and Woessner 1992):

$$S\frac{\partial h}{\partial t} = \nabla \cdot (\boldsymbol{T} \nabla h) + q \tag{1}$$

where h=hydraulic head everywhere in the domain (L); $\boldsymbol{T}$ =second-order tensor of the porous media transmissivity (L^2T^{-1}). It is assumed that $\Delta h \ll h$ so that the saturated depth can be estimated using the hydraulic head: $e \cong h$. S is the specific yield everywhere in the domain; q is the vertical recharge to the saturated surface (LT^{-1}); and "ik" represents different directions in the 2D space according to the principal directions of the tensor $\boldsymbol{T}$.

Integrating the Eq. (1) over the CV V_i (which is indeed a 2D surface control depending on the area of a given mesh element) yields

$$\int\int_{v_i} S_s \frac{\partial h}{\partial t} dv_i = \int\int_{v_i} \nabla \cdot (\boldsymbol{T} \nabla h) dv_i + \int\int_{v_i} q_i dv_i \tag{2}$$

The application of the divergence theorem (or Green's theorem) on the CV V_i yields

$$S_i \frac{\partial h_i}{\partial t} = \oint_{\Gamma_i} (T_{ik} \nabla h)_{ik} \cdot \boldsymbol{n}_{ik} d\lambda + q_i \tag{3}$$

where $q_i = \int\int_{v_i} q dv_i$

$$\int\int_{v_i} S\frac{\partial h}{\partial t} = \int\int_{v_i} S_i \frac{\partial h_i}{\partial t} \tag{4}$$

with $S_i = S\ A_i$ (L^3L^{-1}); and

$$h_i = \frac{1}{A_i}\int\int_{v_i} h dv_i \tag{5}$$

h_i=averages (over the CV) of the hydraulic head (L); Γ_i =contour of the mesh element V_i (L) and $d\lambda$ its elementary variation (L); A_i=surface (L^2) of the mesh element V_i on the horizontal plan; and T_{ik}=transmissivity at the interface between the mesh elements V_i and V_k. It is computed as the product of the saturated hydraulic conductivity (K_{ik}) and the saturated depth (e) of the porous media ($T_{ik}=K_{ik}e$).

Since no approximation has been applied, Eq. (3) is exact. Its discretization on an unstructured and irregular mesh yields

$$S_i \frac{\partial h_i}{\partial t} = \sum \{(T_{ik} \nabla h)_{ik} \cdot \boldsymbol{n}_{ik}\}_{F_{ik}} L_{ik} + q_i \tag{6}$$

Eq. (6) is a second-order approximation in space if the expression "$(T_{ik}\nabla h)_{ik} \cdot \boldsymbol{n}_{ik}$" is accurately evaluated at the midpoint (F_{ik}) of the interface (Murthy and Mathur 1998; Turkel 1985). L_{ik} is the length (L) of the interface between V_i and its adjacent mesh cell V_k. Considering the time integral from time step "$n\Delta t$" to time step "$(n+1)\Delta t$," at interior nodes, Eq. (6) can be written as

$$S_i \frac{(h_i^{(t+1)} - h_i^t)}{\Delta t} = \sum_{k=1}^{N_{vi}} (T_{ik} \nabla h)_{F_{ik}} \cdot \boldsymbol{n}_{ik} L_{ik} + q_i \tag{7}$$

where Δt=time interval (T). If some interfaces of the volumes are boundaries of the study domain, Eq. (7) can be formulated as

$$\frac{S_i}{\Delta t}(h_i^{(t+1)} - h_i^t) = \sum_{k=1}^{N_{vi}} (T_{ik} \nabla h)_{F_{ik}} \cdot \boldsymbol{n}_{ik} L_{ik} + \sum_{b=1}^{N_{ib}} (T_{ib} \nabla h)_{F_{ib}} \cdot \boldsymbol{n}_{ib} L_{ib} + q_i \tag{8}$$

where N_{vi}=number of interior adjacent nodes and N_{ib}=number of boundary faces. The expression "$(T_{ik}\nabla h)_{Fik} \cdot \boldsymbol{n}_{ik}$" in Eqs. (7) and (8) is the flux term through the interfaces between adjacent mesh cells V_i and V_k.

Flux Term Approximation

The admissible geometry of a particular mesh cell (V_i) for the depicted numerical scheme must be a convex geometry configuration. Fig. 2(a) shows an example of a typical mesh cell interface ($\overline{AB}$). The following notation was used in the context of this study (see also the nomenclature at the beginning of the manuscript).

The unit vector $\boldsymbol{n}_{ik}$ is the outward normal unit vector of the interface between V_i and V_k ($\overline{AB}$) and is perpendicular to the unit vector $\boldsymbol{u}_{ik}$. The unit vector $\boldsymbol{v}_{ik}$ joins the midpoint of the adjacent mesh cells (respectively, X_i and X_k). F_{ik} is the midpoint of the interface ($\overline{AB}$). $\boldsymbol{R}_{ik}$ is the intersection of the vectors $\boldsymbol{u}_{ik}$ and $\boldsymbol{v}_{ik}$. θ_{ik} is the angle between the vector $\boldsymbol{n}_{ik}$ and $\boldsymbol{v}_{ik}$. M_i and M_k are the projection points of the adjacent meshes midpoint (respectively,

J. Hydrol. Eng. 2011.16:108-125.

X_i and X_k) on the normal to the interface, including the midpoint F_{ik}. $\boldsymbol{s}_i$ is the unit vector from X_i to M_i. and $\boldsymbol{m}_k$ is the unit vector from X_k to M_k

Several techniques exist for the flux term approximation (Jayantha 2005; Jayantha and Turner 2001, 2003a,b; Turner and Ferguson 1995). The most popular is the two-node method. It is useful for orthogonal meshes: square and rectangular. For nonorthogonal and unstructured meshes, the methods of flux through a representative point of the face (FR) and the technique of the flux through the midpoint of the face (FM) were introduced to improve the accuracy (Jayantha 2005; Jayantha and Turner 2001; 2003a,b; Turner and Ferguson 1995). This last method was used in the BOUSS2D model.

The FM method is based on the directional derivative approximation. The flux at the meshes interface is approximated by the flux in the direction $\boldsymbol{n}_{ik}$. The flux term can be written as

$$(\nabla h_{F_{ik}}) \cdot \boldsymbol{n}_{ik} \approx \frac{1}{\|\boldsymbol{M_i M_k}\|}(h_{M_k} - h_{M_i}) \tag{9}$$

where h_{Mi} and h_{Mk}=hydraulic head at the point M_i and M_k $\|\boldsymbol{M_i M_k}\|$=distance between the point M_i and M_k.

h_{Mi} and h_{Mk} are expressed as follows:

$$h_{M_i} = h_i + (\nabla h)_i \cdot \boldsymbol{s}_i \quad \text{and} \quad h_{M_k} = h_k + (\nabla h)_k \cdot \boldsymbol{m}_k \tag{10}$$

Substitution of Eq. (10) into Eq. (9) yields the following equation for the flux at the interface:

$$(\nabla h_{F_{ik}}) \cdot n_{ik} \approx \frac{1}{\|\boldsymbol{M_i M_k}\|}(h_k - h_i) + \frac{1}{\|\boldsymbol{M_i M_k}\|}[(\nabla h)_k \cdot \boldsymbol{m}_k - (\nabla h)_i \cdot \boldsymbol{s}_i] \tag{11}$$

As shown in Eq. (11), the evaluation of the flux term using the FM method requires an approximation of a local gradient at the mesh nodes $(\nabla h)_i$ as depicted in the forthcoming section.

Approximation of the Local Gradient

Several numerical techniques allow providing a gradient approximation at the mesh nodes. They are based on a variant of the divergence theorem called Green Gauss reconstruction (Barth 1994) cited by (Jayantha and Turner 2001). Using this reconstruction method the local gradient $(\nabla h)_i$ can be estimated using

$$(\nabla h)_i \approx \frac{1}{A_i}\sum_{n=1}^{N_{vi}} h_{F_{ik}} \boldsymbol{n}_{ik} L_{ik} \tag{12}$$

This approximation is also second order as F_{ik} is the midpoint of the interface ($\overline{AB}$) (Murthy and Mathur 1998; Turkel 1985). Several approximation techniques exist (Jayantha and Turner 2001). The most widely used methods are: gradient using a representative point of the face (GRF), least-squares gradient reconstruction or gradient reconstruction using the midpoint of the face for FM (GMF). The latter method of gradient reconstruction (i.e., GMF) is used for the BOUSS2D model.

The hydraulic head at the interface h_{Fik} is evaluated using the gradient through the direction of $\boldsymbol{n}_{ik}$. Assuming the following expressions for the hydraulic head at the interface:

$$h_{F_{ik}} = \alpha_{ik} h_k + (1 - \alpha_{ik}) h_{M_k} \quad \text{or} \quad h_{F_{ik}} = \alpha_{ik} h_i + (1 - \alpha_{ik}) h_{M_i} \tag{13}$$

where α_{ik} is evaluated using the following geometric expression:

$$\frac{(1 - \alpha_{ik})}{\alpha_{ik}} = \frac{\|\boldsymbol{M_i F_{ik}}\|}{\|\boldsymbol{F_{ik} M_k}\|} = \frac{\|\boldsymbol{X_i R_{ik}}\|}{\|\boldsymbol{R_{ik} X_k}\|} \tag{14}$$

The gradient approximation can be expressed as

$$(\nabla h)_i \approx \frac{\Lambda_i^{-1}}{A_i}\sum_{k=1}^{N_{vi}} [\alpha_{ik} h_i + (1 - \alpha) h_k + (1 - \alpha_{ik})(\nabla h)_k \cdot \boldsymbol{m}_k] \boldsymbol{n}_{ik} L_{ik} \tag{15}$$

where $(\nabla h)_k$ is evaluated using the gradient information of the neighboring nodes at only the previous time step; $\boldsymbol{\Lambda_i^{-1}}$ is a matrix of geometric parameters expressed as

$$\Lambda_i = \boldsymbol{I} - \frac{1}{A_i}\sum_{k=1}^{N_{vi}} \alpha_{ik} L_{ik} \boldsymbol{n}_{ik} \cdot (\boldsymbol{s}_i)^T \tag{16}$$

$\boldsymbol{I}$=identity matrix.

Linear System Construction

The above described discretisation procedure produces a set of equations allowing the construction of a linear system at the computational nodes i in the following form:

$$\beta_i h_i = \sum_{k=1}^{N_{vi}} \beta_k h_k + c_i \tag{17}$$

After replacing the flux term expression of Eq. (11) into Eq. (7) and after using the gradient approximation depicted in Eq. (15), the linear system expression can be written as:

$$\frac{S_i}{\Delta t}(h_i^{(t+1)} - h_i^t) = \sum_{p=1}^{N_{vi}} \frac{T_{ik}^{(t+1)} L_{ik}}{\|\boldsymbol{M_i M_k}\|}(h_k^{(t+1)} - h_i^{(t+1)}) + \sum_{p=1}^{N_{vi}} \frac{T_{ik}^{(t+1)} L_{ik}}{\|\boldsymbol{M_i M_k}\|}[(\nabla h)_k^{(t+1)} \cdot \boldsymbol{m}_k - (\nabla h)_i^{(t+1)} \cdot \boldsymbol{s}_k] + q_i \tag{18}$$

The expression $(\nabla h)_k$ at the $(t+1)$th time step was replaced by the gradient at the tth time. Eq. (18) is valid for the interior nodes. The transmissivity at the interface (T_{ik}) was evaluated using the harmonic mean of the transmissivity of adjacent mesh cells (T_i and T_k), as given by the following equation:

$$T_{ik} = \frac{2 T_i T_k}{T_i + T_k} \tag{19}$$

The harmonic mean allows handling the interface transmissivity between adjacent meshes with contrasted soil properties, by avoiding the smoothing effects of the arithmetic mean (Anderson and Woessner 1992).

BCs and Vertical Heterogeneity Handling

Two kinds of boundary condition (BC) are taken into account in the BOUSS2D model: imposed hydraulic head at the boundary (Dirichlet BC), and imposed flux on the domain boundary (Neumann BC). The gradient was approximated at the boundary node. Thus for the node located at the boundary, the Eq. (18) takes the following form:

J. Hydrol. Eng. 2011.16:108-125.

$$\frac{S_i}{\Delta t}(h_i^{(t+1)} - h_i^t) = \sum_{k=1}^{N_{vi}} \frac{T_{ik}^{(t+1)} L_{ik}}{\|\boldsymbol{M_i M_k}\|}(h_k^{(t+1)} - h_i^{(t+1)}) + \sum_{k=1}^{N_{vi}} \frac{T_{ik}^{(t+1)} L_{ik}}{\|\boldsymbol{M_i M_k}\|}[(\nabla h)_k^{(t+1)} \cdot \boldsymbol{m}_k - (\nabla h)_i^{(t+1)} \cdot \boldsymbol{s}_k] + \sum_{b=1}^{N_{ib}} T_i (\nabla h)_{F_{ib}} \cdot \boldsymbol{n}_{ib} L_{ib} + q_i \quad (20)$$

where F_{ib}=center of the boundary segment of the current mesh V_i; L_{ib}=length of the boundary segment; N_{ib}=number of boundary segments surrounding the current mesh; $\boldsymbol{n}_{ib}$=vector outward from the mesh V_i to the boundary segment [see Fig. 2(b)].

Dirichlet BC: Imposed Hydraulic Head

The flux at interfaces of the boundary node depends on the imposed hydraulic head at the boundary of the mesh. Similar to Eq. (9), the flux at the boundary was approximated by the flux through the midpoint of the boundary, using the following expression:

$$(\nabla h_{F_{ib}}) \cdot \boldsymbol{n}_{ib} \approx \frac{1}{\|\boldsymbol{r}_{ib}\|}(h_b - h_{M_i}) \quad (21)$$

The hydraulic head value at the node h_{Mi} is given by Eq. (10). The flux at the boundary can then be expressed as

$$(\nabla h_{F_{ib}}) \cdot \boldsymbol{n}_{ib} \approx \frac{1}{\|\boldsymbol{r}_{ib}\|}[h_b - h_i + (\nabla h)_i \cdot \boldsymbol{s}_b] \quad (22)$$

where the node gradient $(\nabla h)_i$ is expressed as follows:

$$(\nabla h)_i \approx \frac{\Lambda_i^{-1}}{A_i} \sum_{n=1}^{N_{vi}} [\alpha_{ik} h_i + (1-\alpha) h_k + (1-\alpha_{ik})(\nabla h)_k \cdot \boldsymbol{m}_k] \boldsymbol{n}_{ik} L_{ik} + \frac{\Lambda_i^{-1}}{A_i} \sum_{b=1}^{N_{ib}} h_b \boldsymbol{n}_{ib} L_{ib} \quad (23)$$

The linear system for the boundary node can then be written as

$$\frac{S_i}{\Delta t}(h_i^{(t+1)} - h_i^t) = \sum_{k=1}^{N_{vi}} \frac{T_{ik}^{(t+1)} L_{ik}}{\|\boldsymbol{M_i M_k}\|}(h_k^{(t+1)} - h_i^{(t+1)}) + \sum_{k=1}^{N_{vi}} \frac{T_{ik}^{(t+1)} L_{ik}}{\|\boldsymbol{M_i M_k}\|}[(\nabla h)_k^{(t+1)} \cdot \boldsymbol{m}_k - (\nabla h)_i^{(t+1)} \cdot \boldsymbol{s}_k] + \sum_{b=1}^{N_{ib}} T_i \frac{1}{\|\boldsymbol{r}_{ib}\|}[h_b - h_i + (\nabla h)_i \cdot \boldsymbol{s}_b] L_{ib} + q_i \quad (24)$$

Neumann BC: Imposed Flux

Assuming that q_b is the flux through a boundary segment, the linear system can be written as

$$\frac{S_i}{\Delta t}(h_i^{(t+1)} - h_i^t) = \sum_{k=1}^{N_{vi}} \frac{T_{ik}^{(t+1)} L_{ik}}{\|\boldsymbol{M_i M_k}\|}(h_k^{(t+1)} - h_i^{(t+1)}) + \sum_{k=1}^{N_{vi}} \frac{T_{ik}^{(t+1)} L_{ik}}{\|\boldsymbol{M_i M_k}\|}[(\nabla h)_k^{(t+1)} \cdot \boldsymbol{m}_k - (\nabla h)_i^{(t+1)} \cdot \boldsymbol{s}_k] + \sum_{b=1}^{N_{ib}} q_{ib} L_{ib} + q_i \quad (25)$$

The gradient at the boundary nodes is approximated using the equivalent hydraulic head at the boundary. The later is estimated by using the gradient expression similar to Eq. (9)

$$(\nabla h_{F_{ib}}) \cdot \boldsymbol{n}_{ib} \approx \frac{h_{F_{ib}} - h_{M_i}}{\|\boldsymbol{r}_{ib}\|} = q_b / T_{ib} \quad \text{with} \quad h_{F_b} = h_i + (\nabla h)_i \cdot \boldsymbol{s}_b + \frac{q_b \|\boldsymbol{r}_{ib}\|}{T_{ib}} \quad (26)$$

Vertical Heterogeneity Handling

Although the model BOUSS2D is a 2D model, the vertical heterogeneity of the soil matrix can be taken into account. The transmissivity of each mesh element (is computed using the vertical heterogeneity of the soil matrix. For each CV, the transmissivity T_i was evaluated using the following expression (de Marsily 1981):

$$T_i = \int^{e_i} K_j dz \quad (27)$$

where K_j=hydraulic conductivity of the jth soil layer (LT^{-1}), and e_j the thickness of the layer j. Equation (27) was expressed in the following discrete form:

$$T_i = \sum_{j=1}^{N_l} K_j e_j \quad (28)$$

where N_l=number of soil layers.

Matrix Method for Linear System Solving

Eq. (18) or Eq. (20) are used for all the nodes of the domain to form a sparse linear system of N_{vi} variables. The set of resulting equations, after rearranging the terms, can be written using the following matrix formulation:

$$\boldsymbol{A} \cdot \boldsymbol{h} = \boldsymbol{b} \quad (29)$$

with $\boldsymbol{A}$ being a square $N_{vi} \times N_{vi}$ sparse matrix; $\boldsymbol{h}$ being the vector of the N_{vi} hydraulic head variables (h_i) of the domain; and $\boldsymbol{b}$ being the second member vector of the equation. The system can be solved using numerical methods dedicated to this class of matrices, as depicted later in the text.

Model Implementation and Verification Tests

Model Implementation

The BOUSS2D model was implemented as a module of an integrated hydrological modeling framework called LIQUID (Viallet et al. 2006) that is currently under development. The LIQUID framework uses object-oriented programming principles in C++. It includes a *library of modules* describing various hydrological processes, *data input/output facilities*, such as connections with a database and a geographical information systems (GIS) module. A core component handles the temporal connections between modules and manages the time course of the simulations.

A module within the LIQUID framework is made of three components: a preprocessing, a data set and a solver. The *preprocessing* component establishes the link between the database and the GIS to provide a *data set* in the required format for the solver component, particularly for the computational mesh. The *solver* computes the physical process and updates the state variables of

J. Hydrol. Eng. 2011.16:108-125.

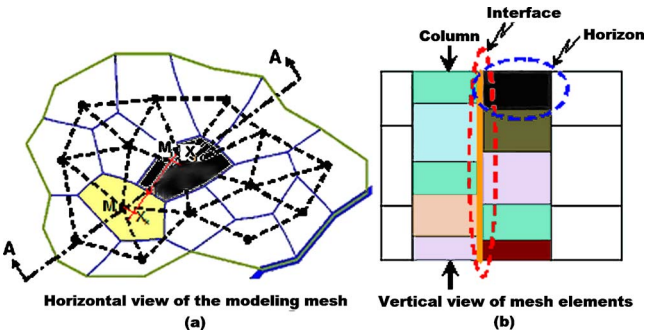

Fig. 3. Objects implemented in the BOUSS2D: (a) example of modeling mesh; (b) vertical vue of mesh element at AA′ profile that illustrates the concepts of column, horizon

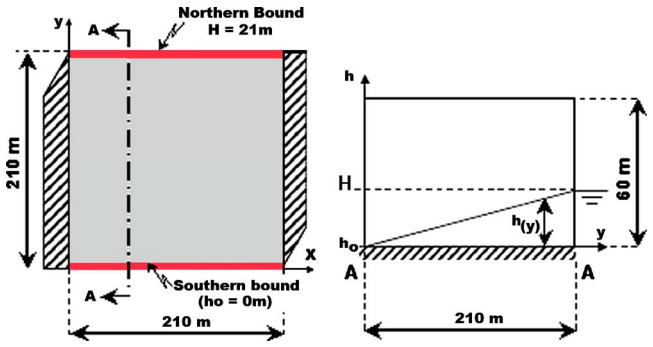

Fig. 4. Characteristics of the modeling domain and BCs considered in test Cases 1-1 and 1-2: (a) horizontal view; (b) vertical profile AA′

the module. The modular structure ensures that the modeler can use the geometry and the numerical scheme he wishes.

For the BOUSS2D module, the objects presented in Fig. 3 were defined using object-oriented programming. The numerical methods depicted in this manuscript were implemented, to calculate the fluxes and gradients occurring within the soil columns. The resolution of the sparse linear system was achieved using the iterative method for symmetric successive over-relaxation method preconditioned bi-CGSTAB (van der Vorst 1992). The Matrix Template Library (Siek and Lumsdaine 1998a; Siek and Lumsdaine 1998b) was used for matrix data structure. The Iterative Template Library (Siek et al. 1998) for algebra routines was used to resolve the linear system.

Numeric Tests for Model Verification

The model was run for several groundwater flow configurations, considering a simplified unconfined aquifer. The verification process was applied to check the accuracy of the chosen algorithms. The method for the verification process was based on the comparison of the BOUSS2D predictions with (1) analytical solutions for simple cases and (2) predictions from other groundwater models for more complicated cases for which no analytical solutions exist or are difficult to derive.

The implemented verification tests were carried out in two consecutive phases. In the first phase, a homogeneous aquifer was modeled to allow the comparison of BOUSS2D prediction with analytical solutions. The groundwater flow through an aquifer caused by a single pumping well was simulated. In the second phase a nonhomogeneous and anisotropic porous media was simulated. The predictions were compared to analytical solutions whenever feasible and to predictions from the well known 3D groundwater models MODFLOW (McDonald and Harbaugh 1988) and MIKE SHE (Abbott et al. 1986a,b). The capability of the model to handle both horizontal and vertical heterogeneities of the porous media was also tested (full tensor conductivity), considering heterogeneous aquifers (discontinuous horizontal permeability) and layered aquifers. The ability of BOUSS2D to handle complex geometries (convex) and discontinuities was also tested.

The model performance was evaluated qualitatively, through visual inspection of suitable plots, and quantitatively through statistical evaluation criteria. The statistical criteria used in the model verification were the RMS error (RMSE), the relative error (RE), and the maximum error (ME). The RMSE was calculated using the formula

$$\text{RMSE} = \sqrt{\frac{\sum_{i}^{N} (h_i - h^{\text{ref}})^2}{N}} \tag{30}$$

where N=number of simulated values; h^{ref}=reference values (analytical solutions or other model predictions); and h_i =BOUSS2D predictions. The RE was calculated by the expression

$$\text{RE} = \frac{1}{N}\sum_{i=1}^{N} \left| \frac{h_i - h^{\text{ref}}}{h^{\text{ref}}} \right| \tag{31}$$

The ME was calculated by the expression

$$\text{ME} = \max|h_i - h^{\text{ref}}| \tag{32}$$

For an easiest reading of the manuscript, the following sections present the description of the case study together with the corresponding results.

First Verification Phase: Homogenous and Isotropic Aquifer

A 210 m × 210 m horizontal, homogenous, and isotropic unconfined aquifer was considered. The soil parameters are: hydraulic conductivity $(K)=2\times10^{-5}$ m s^{-1}, specific yield (S_s) =0.15 m m^{-1} and porosity (n)=0.45.

Steady State Flow with Constant Hydraulic Head as BC: Sensitivity to the Mesh Resolution (Case 1-1)

At the northern and southern bounds of the domain, different imposed hydraulic heads values were considered (Fig. 4). At the northern bound of the domain, a hydraulic head of $H=h(x,210)$ =21 m was imposed, whereas at the southern bound a hydraulic head of $h_0=h(x,0)=0$ was imposed. No-flow BCs were considered at the remaining eastern and western bounds [i.e., $\partial h/\partial x(0,y)=\partial h/\partial x(210,y)=0$ m]. Vertically, the aquifer has an impermeable bottom boundary, and no recharge was allowed to enter the aquifer through the top. Two nonorthogonal meshes [Figs. 5(a and d)] having coarse and fine resolutions were used. The mean area of the mesh elements was, respectively, 900 m^2 for the coarser resolution and 105 m^2 for the finer resolution. The system's dynamics were simulated until the steady state condition was reached.

J. Hydrol. Eng. 2011.16:108-125.

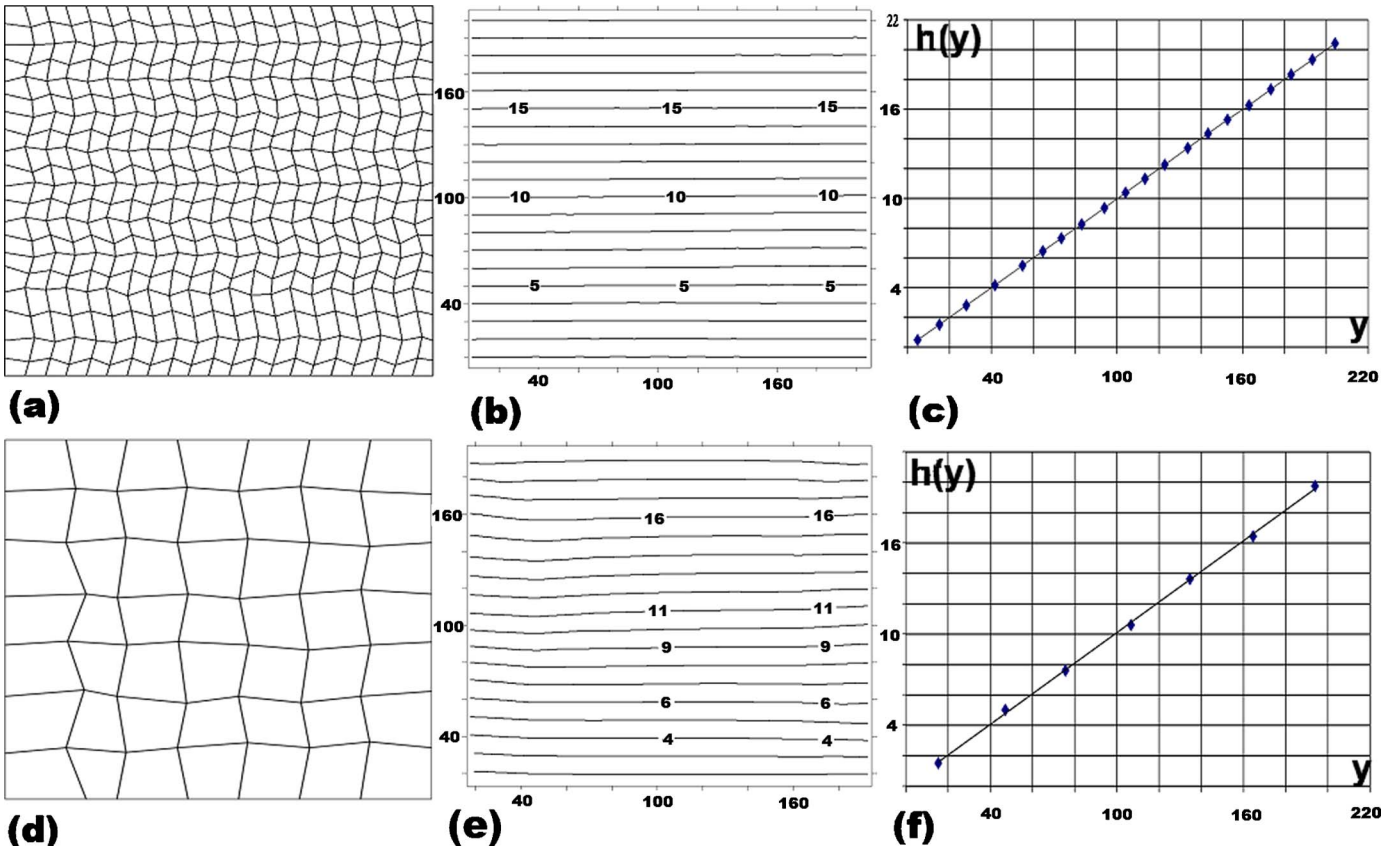

Fig. 5. Different mesh configuration used for Test Case 1-1: (a) average 105-m^2 mesh resolution and (d) average 900 m^2 mesh resolution; (b) and (e) are the predicted spatial distribution of the hydraulic head; and (c) and (f) are the comparison of predicted and analytical hydraulic head values

Under these conditions, there is horizontal flow through the porous media. After reaching the steady state condition, the Laplace equation allows the computation of the hydraulic head everywhere into the domain:

$$\nabla^2 h = 0 \tag{33}$$

Taking into account the BCs described above, the Laplace equation yields

$$\frac{\partial^2 h}{\partial x^2} = 0 \quad \text{thus} \quad \frac{\partial h}{\partial x} = \frac{(H - h_O)}{210} = 0.1 \tag{34}$$

The analytical solution of this equation is therefore

$$h(y) = 0.1y \tag{35}$$

The resulting flow is invariant in the direction parallel to the x-axis and its direction is horizontal. The isolines of hydraulic head are also parallel since they are orthogonal to the flow lines. The steady state predictions of BOUSS2D were compared to the exact analytical solution.

Figs. 5(c and f) present the modeling predictions for the different mesh resolutions. It is shown the mesh configuration, the predicted spatial distribution of the hydraulic head and the graphical comparison of simulated versus analytical value of the predicted hydraulic head. The figure reveals that the BOUSS2D predictions are acceptable, with a good match of the simulated depression profile to the analytical solution, independently of the mesh resolution and despite the use of a nonorthogonal mesh shape. Figs. 5(b and e) shows furthermore that the predicted hydraulic head isolines are parallel as should be. Table 1 summarizes the model performance statistics for the different mesh resolutions. It shows the good agreement between the BOUSS2D predictions and the analytical solution, for both resolutions, since the relative error is below 1%. The statistics show furthermore that the agreement is better for the finer resolution which suggests that the BOUSS2D model is slightly sensitive to the mesh resolution, despite the acceptable accuracy observed in both cases (Table 1).

Steady State Flow with Constant Hydraulic Head as BCs: Sensitivity to the Mesh Shape (Case 1-2)

For this test case, the same aquifer and BCs as the ones considered in the Test Case 1-1 were used (Fig. 4). The imposed hydraulic head was also the same as for the previous test (H =21 m at the northern bound and h_o=0 m at the southern bound). Four mesh shapes, namely square, hexagonal, distorted nonorthogonal and completely unstructured were used to test the robustness of BOUSS2D to handle unstructured meshes [Figs. 6(a, d, g, and j)]. The respective analytical solution is also given by Eq. (35). The flow direction is horizontal, and the hydraulic head isolines are parallel.

Figs. 6(c, f, i, and e) show the BOUSS2D predictions as a function of the used mesh configurations. The figure shows furthermore the simulated spatial distribution of the hydraulic head

Table 1. Model Performance Statistics for Test Case 1-1

Mesh configuration	RE (%)	ME (m)	RMSE (m)
Fine [Fig. 6(a)]	0.0995	0.0024	0.0009

J. Hydrol. Eng. 2011.16:108-125.

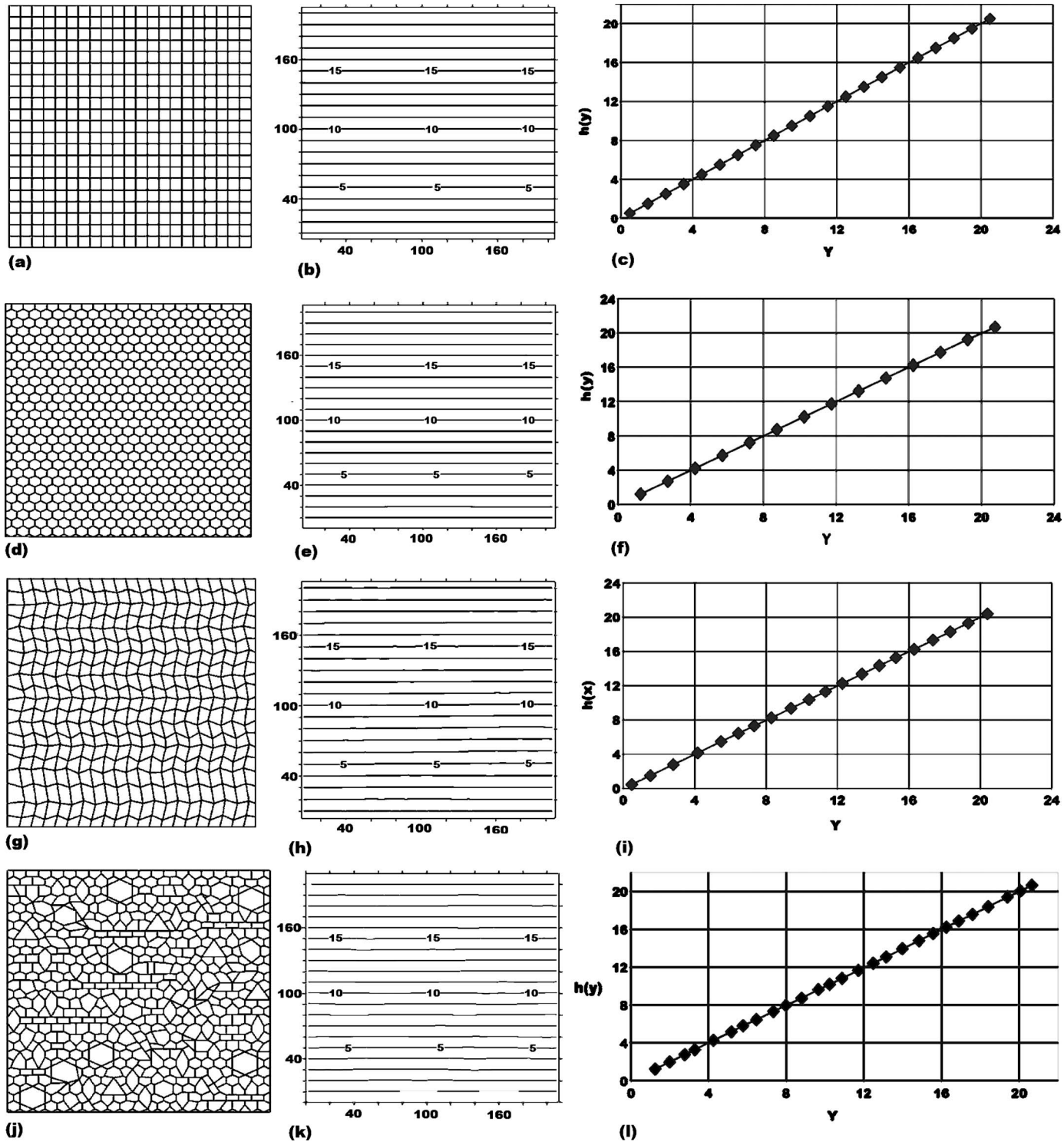

Fig. 6. Different mesh configurations used for Test Case 1-2: (a) a grid; (d) hexagonal mesh; (g) distorted nonorthogonal grid; and (j) random unstructured grid; (b), (e), (h), and (k) are the predicted spatial distribution of the hydraulic head; (c), (f), (i), and (e) are the comparison of predicted and analytical hydraulic head values.

and the respective graphical comparison of simulated versus analytical values. The figure reveals a good agreement of the simulated flow with respect to the exact solution, independently of the mesh shape configuration. All the simulated isolines are parallel to the *x*-axis matching the analytical solution [Figs. 6(b, e, h, and k)]. Table 2 provides a summary of the model performance statistics. It confirms the good agreement of the simulated and ana-

Table 2. Model Performance Statistics for Test Case 1-2

Mesh configuration	RE (%)	ME (m)	RMSE (m)
Square	0	0	0
Hexagonal	6.777×10^{-5}	2.210×10^{-2}	2.018×10^{-2}
Non orthogonal	6.698×10^{-3}	2.411×10^{-3}	6.224×10^{-2}
Unstructured	7.629×10^{-3}	9.298×10^{-2}	3.344×10^{-2}

J. Hydrol. Eng. 2011.16:108-125.

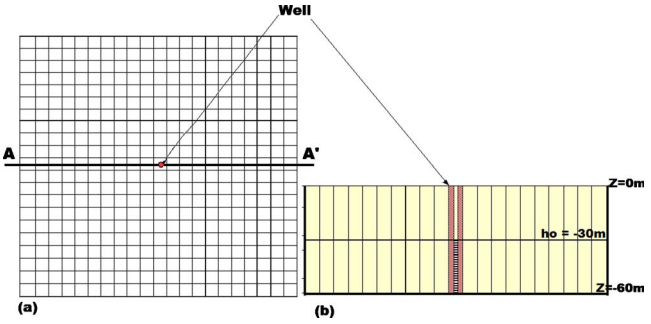

Fig. 7. Simulation domain for a pumping simulation into a homogeneous aquifer (Test Case 1-3)

lytical predictions for all of the meshes. These results stress the robustness of the BOUSS2D numerical structure to handle appropriately various mesh shape configurations, which constitutes by itself a very significant advancement in terms of domain discretization with regards to either the square-grid based or the orthogonal-grid based models.

Single Pumping Well: Comparison of BOUSS2D Predictions with an Analytical Solution and Predictions from Existing Codes (Case 1-3)

The simulation domain (Fig. 7) is an unconfined aquifer with a single pumping well, located at its center. The ground and aquifer bottom elevations are, respectively, $Z_{surf}=0$ m and $Z_{bottom}=-60$ m. The initial hydraulic head was $h_o=-30$ m. The pumping lasted four hours with a constant discharge of $Q=0.001$ m^3 s^{-1}, ensuring a null drawdown at the limit of the domain throughout the pumping. The horizontal aquifer boundaries were given no-flow conditions. The following well and aquifer properties were assumed:

- The well is fully penetrating (over the entire thickness of the aquifer);
- The radius of the well is significantly small (so no significant water volume can be stored into it);
- The aquifer has an infinite extent (implying that the gradient at the domain boundary is zero);
- The aquifer is horizontal (not sloping), and has an impermeable (nonleaky) bottom boundary; and
- The piezometric surface of the aquifer has a small gradient.

Under these conditions, there exists an analytical solution describing the groundwater flow induced by the pumping. As the aquifer is assumed to be homogenous and isotropic, an elementary solution in radial coordinates can be used. The most popular is the Theis solution (de Marsily 1981; Theis 1935). This equation was established initially for confined aquifers but Tison (1953), cited by Castany (1966), demonstrated that it could be used for unconfined aquifers with infinite extent. The Theis solution implies that the transient drawdown form of the well can be expressed as

$$\Delta h(x)=\frac{-Q}{4\pi T}\left[-E_i\left(-\frac{x^2S}{4Tt}\right)\right] \tag{36}$$

where T (L^2T^{-1}) and S=transmissivity and storativity (specific storage multiplied by the groundwater thickness) of the aquifer around the well; x=distance from the pumping well to the point where the drawdown is observed (L); t=time since the pumping started (T); and $E_i(u)$=exponential integral function (or "Well function;" de Marsily 1981). In addition, numeric predictions were produced by using MODFLOW and MIKE SHE for their respective comparison to the BOUSS2D predictions.

Fig. 8 shows the comparison of the water table level simulated using BOUSS2D, MODFLOW and MIKE SHE with respect to the analytical solution, after 4 h of pumping. In general it shows the good agreement between the prediction of the different models (including BOUSS2D) and the analytical solution. Table 3 summarizes the respective model performance statistics calculated with the analytical solution [Eq. (35)] as the reference. The

Table 3. Model Performance Statistics for Test Case 1-3

Code	RE (%)	ME (m)	RMSE (m)
BOUSS2D	$\mathbf{2.20\times10^{-5}}$	**0.0041**	**0.00149**
MODFLOW	7.14×10^{-5}	0.0172	0.00552
MIKESHE	6.32×10^{-5}	0.0162	0.00516

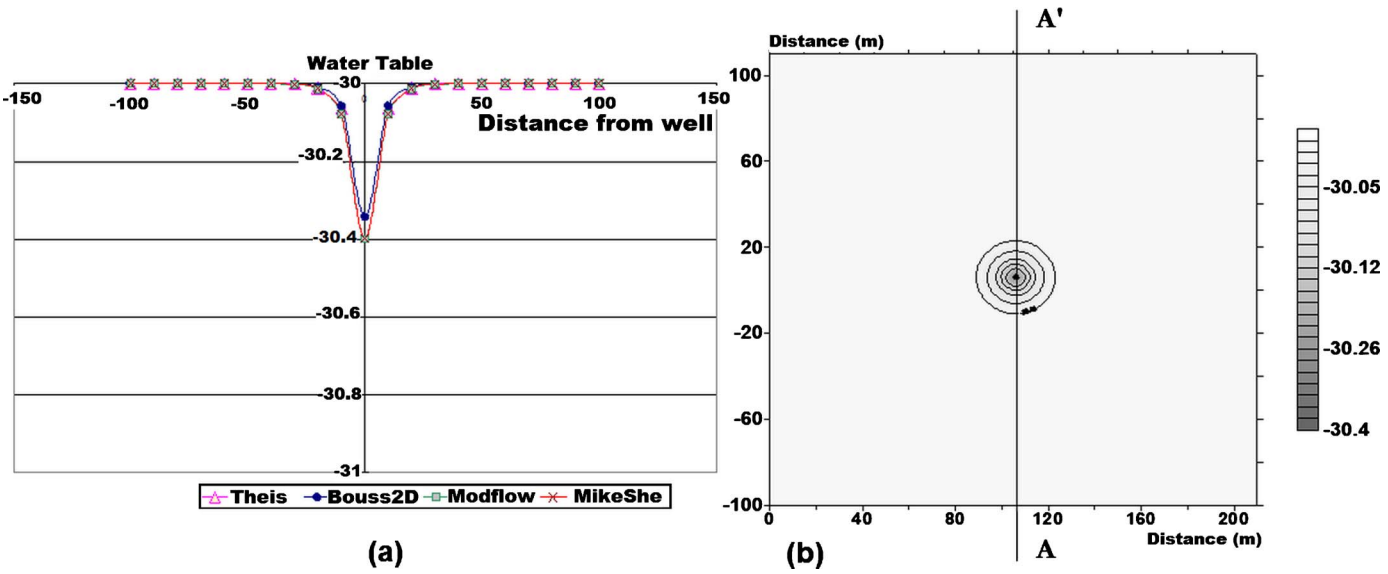

Fig. 8. Hydraulic head drawdown profile after 4 h of pumping (Test Case 1-3): (a) vertical profile; (b) isoline map

J. Hydrol. Eng. 2011.16:108-125.

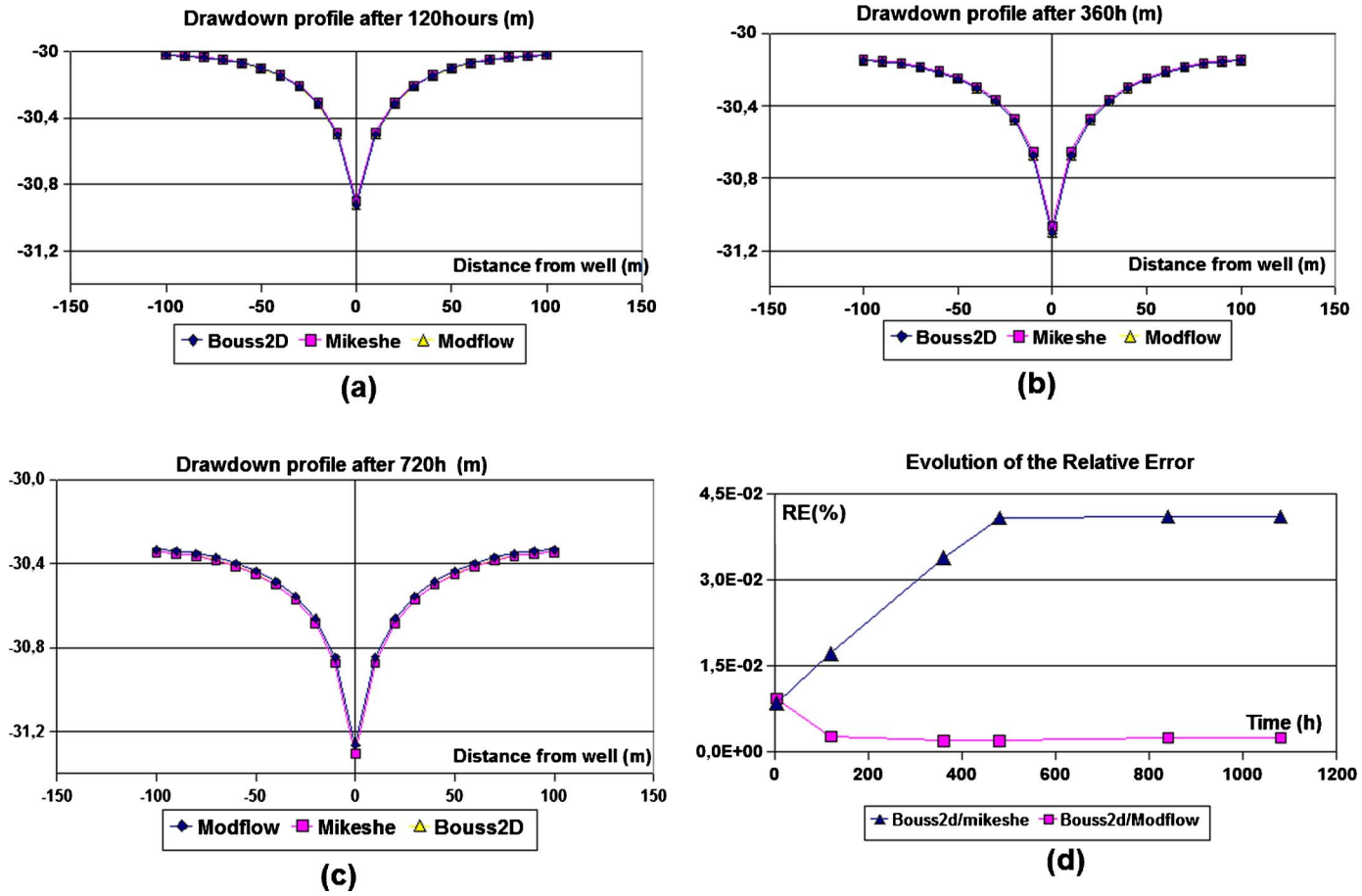

Fig. 9. Comparison between BOUSS2D prediction and the prediction of the reference models at different time step (Test Case 1-3): [(a)–(c)] hydraulic head drawdown; (d) evolution of the relative error

model performance statistics show that BOUSS2D, MODFLOW, and MIKE SHE produce comparable performances.

Considering the same aquifer as in the previous verification test, we extended the pumping duration to two months. Under these conditions, the analytical solution cannot be used anymore because the assumption of the aquifer having an infinite extent is no longer acceptable and there is therefore a significant influence of the BCs on the predictions. The BOUSS2D predictions were therefore only compared with those of the other simulation codes. The head drawdown profiles at different time steps are presented in Figs. 9(a–c). It shows a close agreement between the three models. Fig. 9(d) presents the time evolution of the relative differences between the BOUSS2D model and the reference models. It depicts that in this verification test, the BOUSS2D predictions are more similar to the ones produced by the MODFLOW predictions and that this agreement improves with the simulation time.

Second Verification Phase: Heterogeneous Aquifers

A heterogeneous aquifer, having the same geometric properties as in the previous test cases was used. Different aquifer configurations were considered to represent more realistic modeling conditions. The single pumping well problem was analyzed considering three conditions: (1) an aquifer with a horizontal variation of the permeability; (2) a layered aquifer (vertical variability of permeability); and (3) an aquifer with an embedded flow barrier (significantly contrasting geological materials).

In addition, an even more realistic problem was analyzed with BOUSS2D to simulate the transient groundwater dynamics of a three-layered aquifer system from where water is pumped for supply purposes.

Horizontal Aquifer Heterogeneity: Steady State Flow around a Pumping Well (Case 2-1)

In this section, we evaluate the BOUSS2D capability to handle horizontal variations of permeability. By modeling a pumping well in a heterogeneous aquifer domain formed by alternated coarse and fine sandy materials, implying an important lateral variation of permeability (Fig. 10). This situation represents an alluvial deposit surrounded by a larger unconfined aquifer. The pumping well is located at the center of the domain, in the coarse sandy material. The pumping discharge is $Q=0.012$ m^3 s^{-1}. At steady state conditions, there exists an analytical solution for this type of problem, given by the following equation (Castany 1966):

$$H^2 - h^2(x) = \frac{2Q}{\pi(k_1 + k_2)}\left(\ln\frac{R_1}{x} + \ln\frac{R_2}{R_1}\right) \tag{37}$$

The respective shape of the drawdown profile at the steady state condition is depicted in Fig. 11(a), as given by Eq. (37). The initial water table level was $h_0=-30$ m. The soil material parameters are summarized in Table 4. Three mesh configurations were considered (Fig. 10): square with a resolution of 6 m, square with a resolution of 10 m and completely unstructured mesh. For each mesh configuration, BOUSS2D was run until steady states conditions were reached and the respective predictions were compared

J. Hydrol. Eng. 2011.16:108-125.

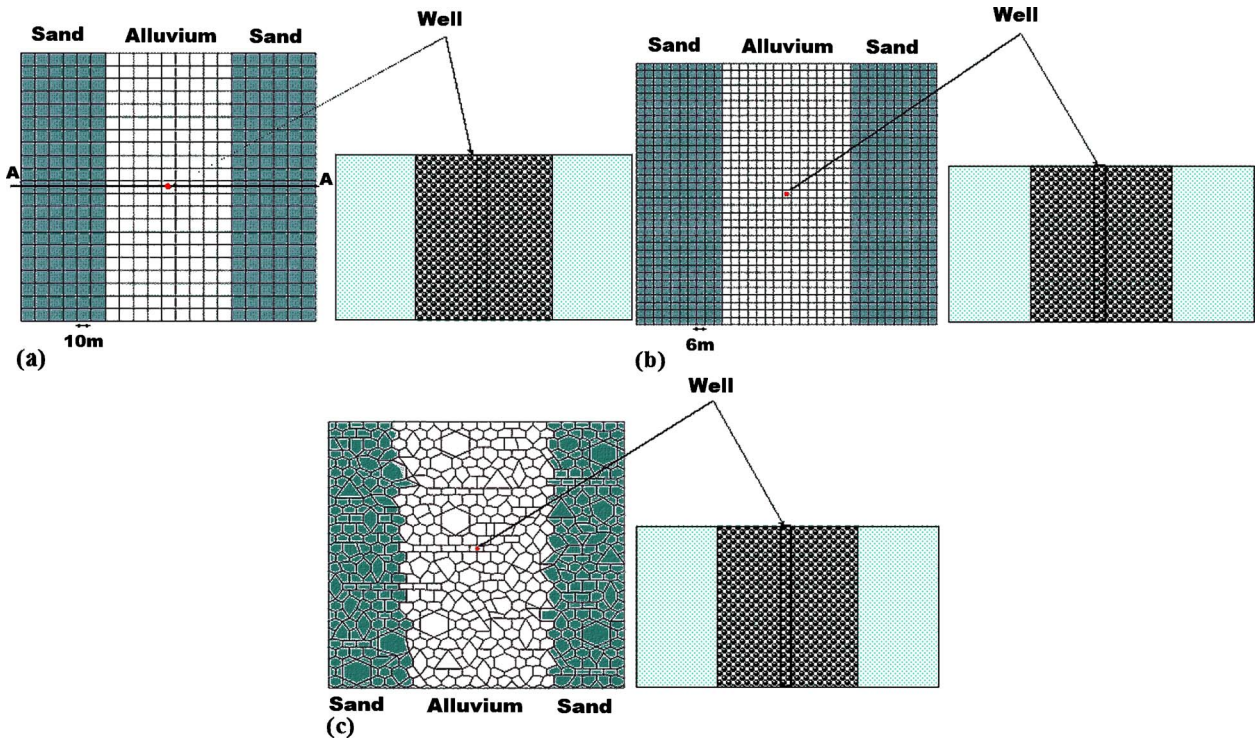

Fig. 10. Simulation domain considered for Test Case 2-1; steady flow around water intake structure on heterogeneous aquifer domain. (a) Mesh resolution is 10 m; (b) mesh resolution is 6 m; and (c) unstructured and irregular mesh.

with both the analytical solution and the predictions from MODFLOW and MIKE SHE.

Fig. 12(a) shows, the comparison between the analytic solution and the BOUSS2D predictions as a function of the different mesh configurations. It suggests in general a good match between the predictions and the analytic head drawdown, independently of the modeling mesh. Furthermore, Table 5 depicts the respective performance statistics, which does not only confirms the acceptable performance of BOUSS2D for all of the considered meshes but also depicts that better predictions were obtained, as expected with the finer (square) resolution. Both Fig. 12(a) and Table 5 suggest that the BOUSS2D performance handling horizontal heterogeneities remains very acceptable even when unstructured meshes are used.

Fig. 12(b) shows moreover the comparison of the analytic solution with respect to the predictions by BOUSS2D, MODFLOW and MIKE SHE, considering the 6-m square mesh configuration. The figure suggests that the performance of BOUSS2D is significantly superior to the performance associated to the other two models. The same was observed when considering the 10 m square mesh configuration. The shape of the head drawdown curves simulated by MODFLOW and MIKE SHE are almost perfectly coincident with each other but exhibits different curvature patterns than the analytic solution. This pitfall was not observed for the BOUSS2D predictions, except for the unstructured mesh case [i.e., Fig.12(a)], but even then the BOUSS2D performance is in general terms better than the 6-m square mesh predictions of MODFLOW and MIKE SHE.

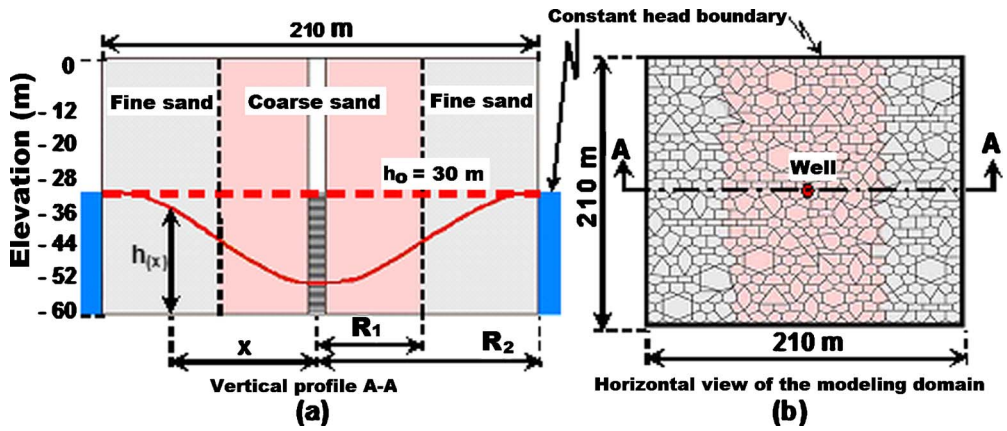

Fig. 11. Characteristics of the modeling domain and BCs used in Test Case 2-1: (a) vertical profile AA′; (b) horizontal view that illustrates the mesh configuration.

J. Hydrol. Eng. 2011.16:108-125.

Table 4. Soil Material Parameters for the Heterogeneous Aquifer Used for Test Case 2-1

Layer identifier	Soil type	K ($m\ s^{-1}$)	S_y	n
1	Alluvium	2.0×10^{-3}	0.2	0.3
2	Fine sand	2.0×10^{-4}	0.15	0.45

Table 5. Model Performance Statistics for Test Case 2-1

Mesh configuration	RMSE (m)	ME (m)	RE (%)
BOUSS2D 10 m	0.0086	0.0202	0.024
BOUSS2D 6 m	0.007	0.0097	0.0002
BOUSS2D unstructured mesh	0.0145	0.0284	0.0004

Layered Aquifers: Comparison with Predictions from Existing Codes (Case 2-2)

The considered aquifer is composed by three vertical geologic layers depicted in Fig. 13. From the top to the bottom, the materials of these layers are: sand (40 m thick), fine sand (10 m thick), and silt (10 m thick). The corresponding soil parameters values are summarized in Table 6. A square mesh with a resolution of 10 m was used.

The initial water table level was fixed as $h_0=-30$ m everywhere in the domain. No recharge was allowed to enter through the top of the aquifer. No-flow BCs were adopted elsewhere at the (vertical and horizontal) bounds of the domain. The pumping discharge was $Q=0.001\ m^3\ s^{-1}$. The BOUSS2D predictions were compared to the respective predictions from MODFLOW and MIKE SHE. A square mesh with a resolution of 10 m was adopted to establish a common comparison basis for the three models, in particular because MIKE SHE can only accept square mesh configurations.

Figs. 14(a–c) shows the evolution throughout time of the head drawdown profile for different simulation time steps when considering a vertically heterogeneous aquifer. Fig. 14(d) suggests that the predictions of hydraulic head from the three models agree with each other. The relative error of the BOUSS2D was about 1×10^{-3} m, as compared to MIKE SHE and about 6×10^{-3} when compared to MODFLOW (Table 7). The comparison reveals a good fitting between the BOUSS2D predictions and those produced by the existing 3D reference models. These results show the capability of BOUSS2D to handle vertical soil media heterogeneities, despite the fact that it is in principle only a 2D model.

Geologic Contrast Embedded in a Homogeneous Aquifer (Case 2-3)

The BOUSSD capability to deal appropriately with very contrasted and unstructured features was evaluated considering a 210 m $\times$ 210 m domain, depicted in Fig. 15. It includes a significant geological contrast (it may be a natural geological intrusion or an artificial structure) embedded in a homogeneous aquifer. The soil parameters values of the homogeneous domain are: $K=2\times10^{-5}\ m\ s^{-1}$, specific yield $S=0.15$ and $n=0.45$. For the geologic intrusion $K=2\times10^{-20}\ m\ s^{-1}$, $S=4\times10^{-5}$ and porosity $n=0.1$. The initial water table level was fixed as $h_0=-30$ m, everywhere in the domain. No-flow BC were adopted at the horizontal bounds of the domain and at the bottom of the modeled aquifer. The pumping discharge was $Q=0.001\ m^3\ s^{-1}$. In this case, we did not compare the results with other models. We only checked the consistency of the simulated behavior.

Fig. 16 shows the spatial distribution of the simulated hydraulic head for different simulation instants. It illustrates the distorting effect of the discontinuity on the spatial distribution of the hydraulic head, as compared to the homogeneous case. It shows that the simulation was realistic and the flows get around the discontinuity. Although no numerical comparisons were carried out, the visual comparison of flow patterns and drawdown values with regard to the MIKE SHE and MODFLOW predictions confirmed that the BOUSS2D performance is very much acceptable. Thus, these analyses suggest that BOUSS2D allows handling a significant spread of modeling conditions with a wide range of flexibility. It is then possible to acceptably handle a natural discontinuity such as geological features, natural water bodies, etc.

Real World Test Case (Case 2-4)

This study case is based on the three-dimensional groundwater modeling reported in the tutorial of the groundwater modeling code Visual Modflow [Schlumberger Water Services (SWS) 2007]. The study site (Fig. 17) is located in the Region of Waterloo (Ontario, Canada). The modeling domain is a $2\times2\ km^2$ aquifer from where water is abstracted through two municipal water supply (fully penetrating) wells that pump constantly a rate of $4.6\times10^{-3}\ m^3\ s^{-1}$ (well 1) $6.4\times10^{-3}\ m^3\ s^{-1}$ (Well 2). The geology at the site consists of an assembling of three layers [Fig.

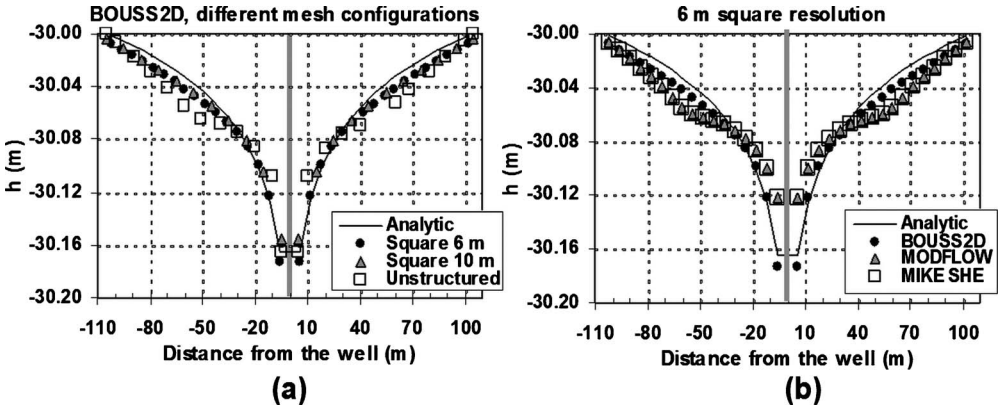

Fig. 12. Test Case 2-1 results: hydraulic head variation along the profile AA: (a) comparison between the BOUSS2D predictions and the analytical solution using different mesh configurations; (b) comparison between the BOUSS2D predictions and the predictions from BOUSS2D, MODFLOW, and MIKE SHE for a grid with 6-m resolution

J. Hydrol. Eng. 2011.16:108-125.

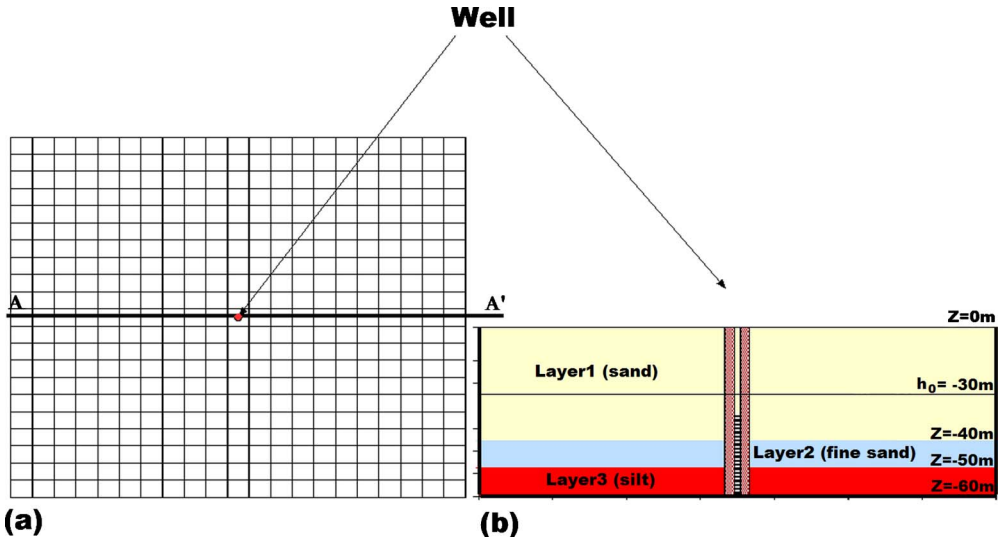

Fig. 13. Characteristics of the modeling domain considered in Test Case 2-2: pumping simulation in a layered aquifer

Table 6. Soil Material Parameters for the Layered Aquifer (Test Case 2-2)

Layer identifier	Soil type	K (m s^{-1})	S_y	n
1	Sand	5.5×10^{-4}	0.3	0.3
2	Fine sand	4.0×10^{-5}	0.32	0.35
3	Silt	5.0×10^{-7}	0.2	0.42

17(b)]. The upper (L1) and lower (L3) layers have higher permeability than the second one (L2), which was modeled as an aquitard separating the upper and lower aquifers. Correspondingly, L1 and L3 have a (isotropic) hydraulic conductivity of 2×10^{-4} m s^{-1}, whilst the aquitard has a (isotropic) conductivity of 1×10^{-10} m s^{-1}. With respect to the physical properties of the geologic materials, the three layers have nearly the same characteristics. Thus, the three layers were modeled considering the following physical properties: S=0.2 and n=0.3.

Both the ground as well as the bottom of the modeled domain are nearly horizontal, whereas the bottom of L1 and L2 are nonhorizontal and significantly variable in space. A transient simulation was set up, considering a pumping period of 270 days and a

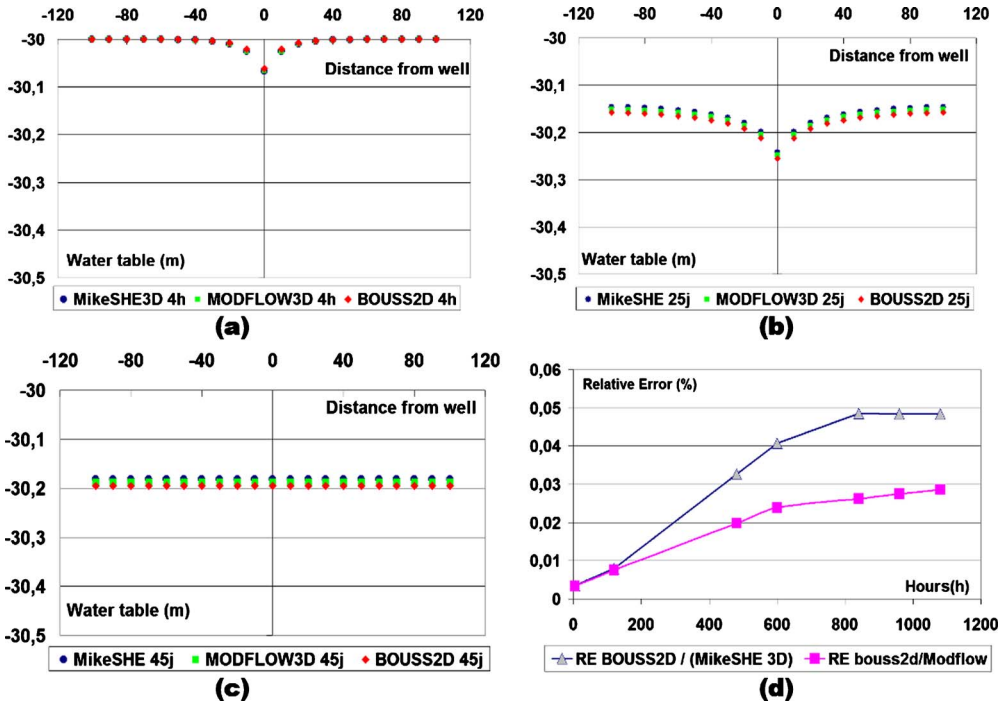

Fig. 14. Hydraulic head drawdown profiles evolution for Test Case 2-2: (a) after 4 h, (b) after 600 h; and (c) after 1,080 h. (d) Relative error as a function of time as compared with MIKE SHE and MODFLOW

J. Hydrol. Eng. 2011.16:108-125.

Table 7. Model Performance Statistics for Test Case 2-2

Reference code	RMSE (m)	ME (m)	RE (%)
MIKE SHE	0.01134	0.00037	0.03096
MODFLOW	0.00657	0.00023	0.01866

posterior recovering period of 95 days until completing a year of analysis. The modeled system includes a river located by the southern boundary of the study site, running from west to east. Since currently BOUSS2D does not include a river-aquifer interaction package (currently under development), the water levels at the river reach were modeled as a constant head BC (Fig. 17) varying in space according to the river gradient. We believe that this is an acceptable approximation given that the purpose of this paper is to illustrate the feasibility of groundwater modeling using unstructured convex grid configurations rather than matching more accurately the dynamics of the modeled system.

The BCs at the remaining horizontal bounds as well as at the bottom of the modeled domain were set up as no flow [Fig. 17(b)]. The same BC was adopted for every modeled layer, so that there is not vertical variation of the BC. Furthermore, a constant recharge of 3.17×10^{-9} m s^{-1} was considered for most of the area [Zone 1; Fig. 17(a)], except for a spot influenced by a structure that is present in the study site [Zone 2; Fig. 17(a)] and that causes a higher recharge to the upper aquifer, in the order of 7.93×10^{-9} m s^{-1}. The initial head was fixed as -5.26 m throughout the whole modeling domain. To judge on the BOUSS2D performance, its predictions were compared to the respective MODFLOW predictions, in particular about the water table level fluctuation and direction of the flow.

Fig. 18 presents the spatial distribution of the hydraulic head predicted by BOUSS2D and MODFLOW for different simulation instants, i.e., 30 days after the beginning of the pumping (Plots a and b), 270 days by the end of the pumping (Plots c and d), and 365 days by the end of the simulation period (Plots d and e). In general, it shows a very acceptable agreement between the predictions of BOUSS2D and MODFLOW. The groundwater flow at each time step is similar for both models despite the fact that the problem that has been herein analyzed implies a significant vertical variation of the hydraulic head, owing not only to the vertical succession of different geological materials with varying geometrical dimensions but particularly to the adopted no-flow condition by the northern boundary of the domain. Under these circumstances, the groundwater flow is significantly three dimensional, despite of which BOUSS2D has achieved an acceptable performance as stressed by Table 8 that depicts that the drawdown relative discrepancy with respect to the one predicted by MODFLOW is only about 3.4%.

Thus, these results suggest that BOUSS2D is capable of handling real world applications, which do not involve important vertical variations of the hydraulic head, given that the current version of BOUSS2D is meant to work under Dupuit conditions, that is, when vertical friction loss is not that significant. Besides applications such as the one depicted herein, the current form of BOUSS2D has the potential of being suitable for the analysis of other groundwater problems such as the one related to civil engineering excavation works, etc.

Discussion

The test cases presented herein showed that BOUSS2D is capable of handling efficiently unstructured and irregular meshes and aquifer vertical and horizontal discontinuities. With the perspective of coupling it with an unsaturated zone water transfer model and a river flow model, this capability is by itself very interesting. When the surface landscape heterogeneity is taken into account (land use, soil, hillslopes, river networks, etc.), the corresponding land surface discretization leads to irregular geometries (Dehotin and Braud 2008). For the building of an integrated model representing vertical water transfer within the soils units, including evapotranspiration, groundwater and river flows, as well as their interaction with rivers, this geometry must be transformed into convex meshes (see Fig. 1). With such a geometry configuration, an efficient coupling between an unsaturated zone module and the groundwater flow BOUSS2D module is expected. In addition, the further development of tools for easing the definition of BCs of aquifers as well as the modeling of the river-aquifer interactions should also be undertaken more easily in the future.

Nevertheless, in its present state, BOUSS2D has still some limitations. The considered gradient approximation method (FM)

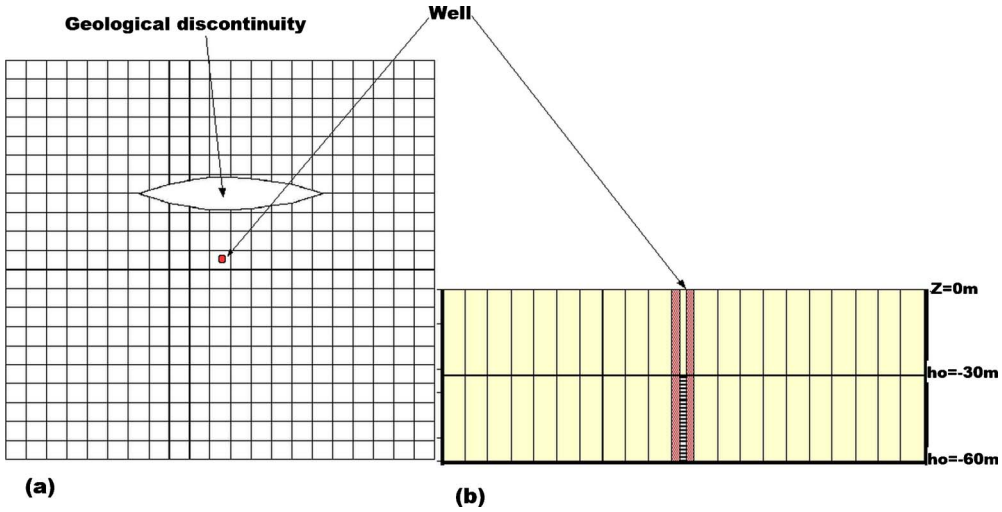

Fig. 15. Mesh configuration and modeling domain characteristics used in Test Case 2-3: geological discontinuity into a homogeneous soil material

J. Hydrol. Eng. 2011.16:108-125.

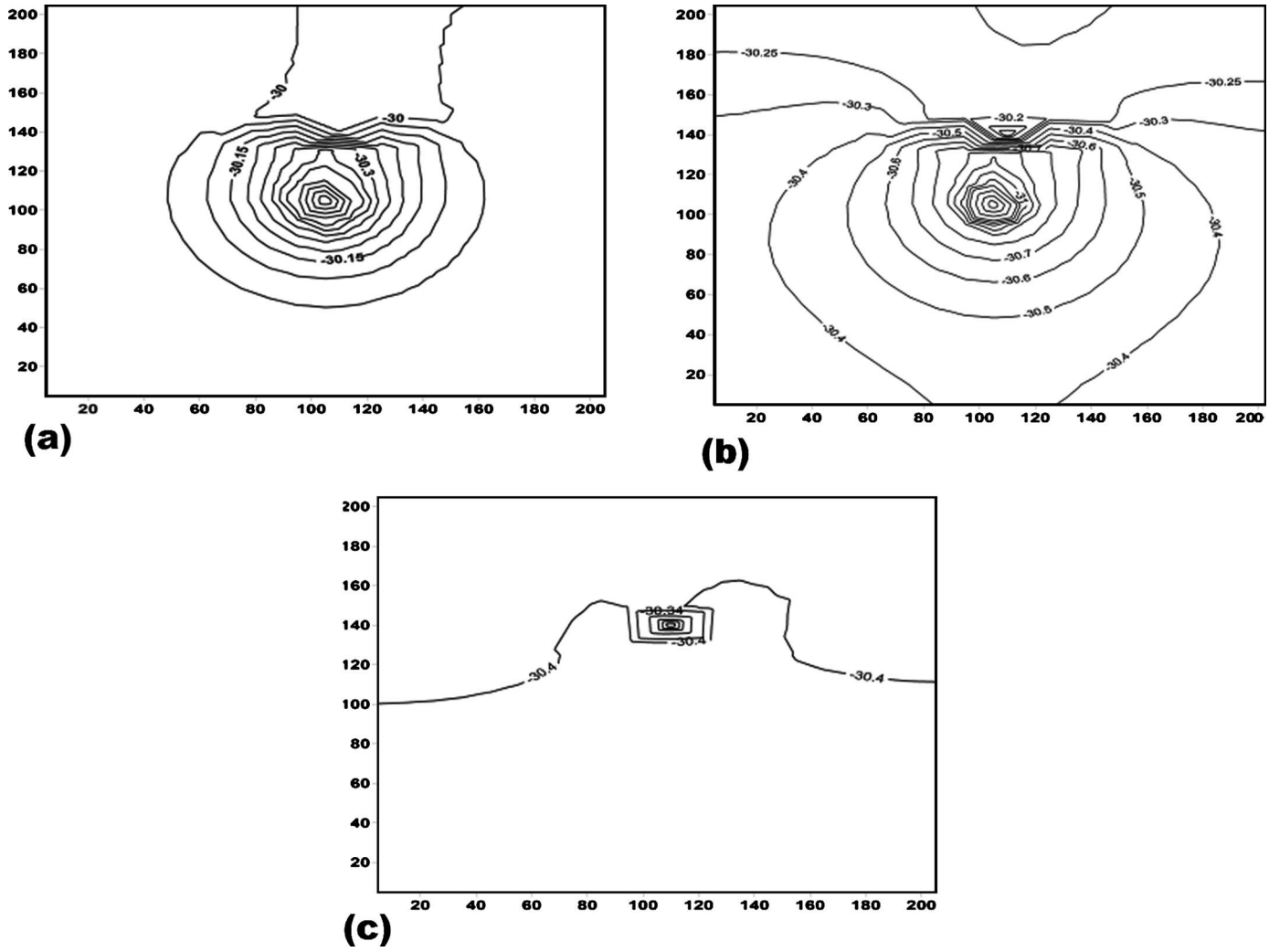

Fig. 16. Spatial distribution of the hydraulic head at different time step (Test Case 2-3): (a) 3, (b) 30; and (c) 60 days

introduces a geometrical constraint related to the projected points (M_i and M_k) used as representative of the mesh element (the points must be inside the mesh). So, the test on highly nonorthogonal meshes such as the Kershaw grid was not conclusive because of the gradient approximation method (see an example in Loudyi et al. 2007). The Kershaw grids do not verify the latter geometrical constraint. The improved least squares gradient reconstruction method in Loudyi et al. (2007) is able to handle this

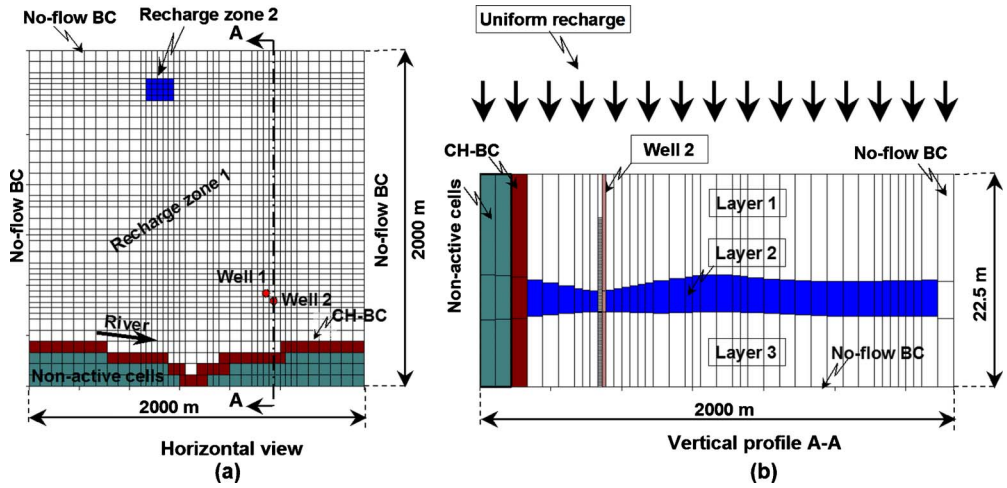

Fig. 17. Characteristics of the modeling domain considered in Test Case 2-4: real world test case

J. Hydrol. Eng. 2011.16:108-125.

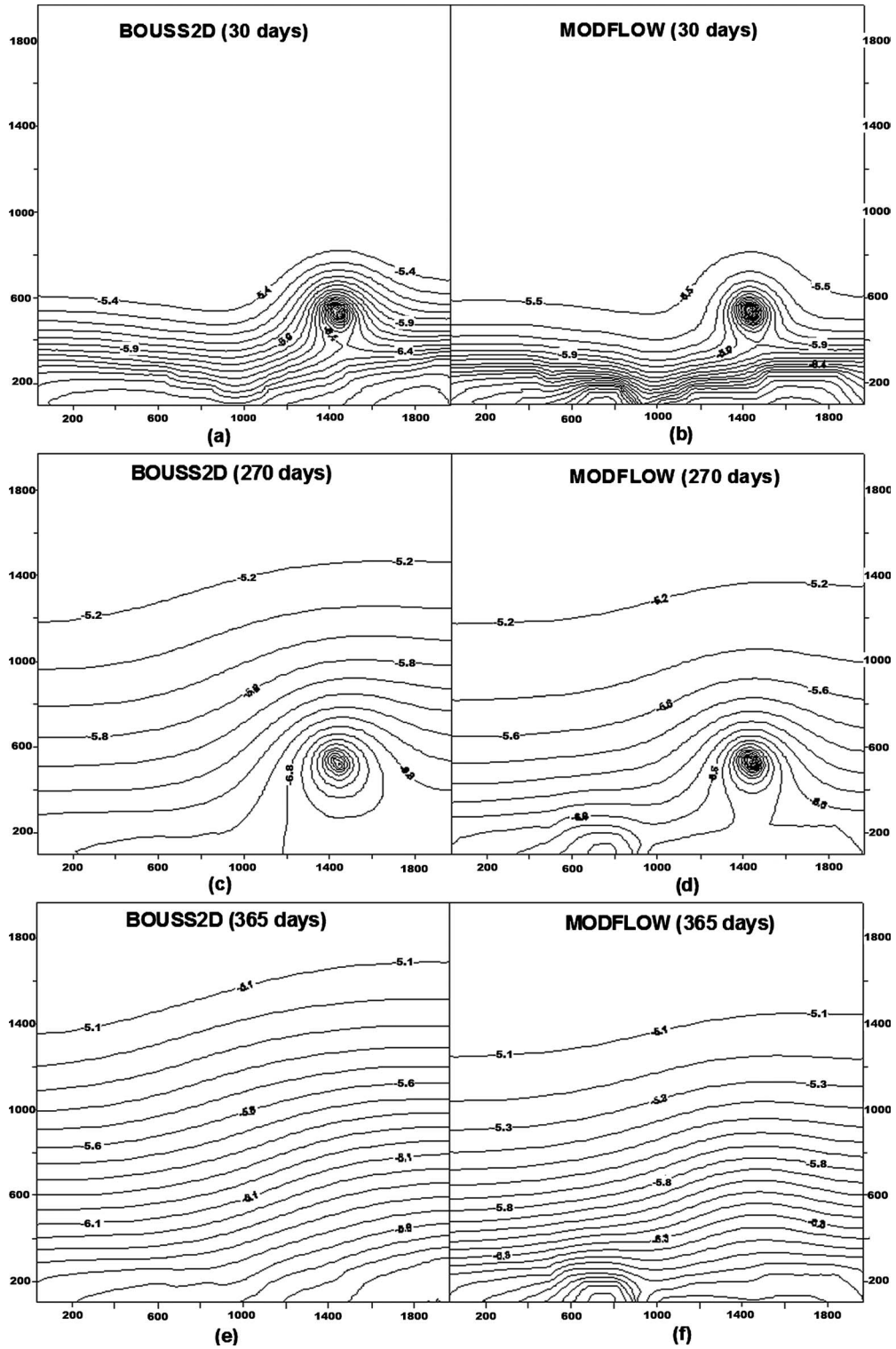

Fig. 18. Spatial distribution of the predicted hydraulic head at different modeling time steps (Test Case 2-4) for [(a), (c), and (e)] BOUSS2D; [(b), (d), and (f)] MODFLOW

Table 8. Model Performance Statistics for Test Case 2-4

Reference code	RMSE (m)	ME (m)	RE (%)
MODFLOW	0.219797818	0.725210743	3.449102124

Kershaw geometry but it is restricted to quadrangular unstructured meshes. The combination of the BOUSS2D and the Loudyi et al. (2007) methods could provide a more general solution to the problem. It is also important to mention that the mesh geometric configuration must be convex to be suitable for the numerical scheme used. This problem may also be overcome using another gradient approximation method such as the least squares gradient

reconstruction method or the multipoint methods.

Test Cases 2-2 and 2-4 showed that BOUSS2D is able to handle some vertical heterogeneity. However complex vertical heterogeneities cannot be accounted for as with fully three-dimensional models because the vertical friction loss is not taken into account. BOUSS2D must in principle be used only when the Dupuit condition is fulfilled. Further verifications and comparisons with 3D codes should be carried out in the future to determine to what extent the BOUSS2D approximations can lead to acceptable predictions, whenever the Dupuit hypothesis is not fulfilled.

Conclusions and Perspectives

In this paper, we illustrate how groundwater processes can be modeled using unstructured meshes. The BOUSS2D model is a new model for groundwater flow simulation that allows the use of these irregular and unstructured meshes. It was run with a variety of groundwater flow configurations, and varied mesh shapes and sizes. A simple pumping test simulation in a homogeneous aquifer was used to verify the model results by comparing with an analytical solution and the predictions from the MODFLOW and MIKESHE codes, taken as reference models. The analyses demonstrated the accuracy of the BOUSS2D model. A good agreement with both the analytical solution as well as the predictions from the reference models was observed. The capability of the BOUSS2D model to take into account vertical heterogeneities was evaluated using a pumping simulation on layered aquifers. The results showed the accuracy of the BOUSS2D model as compared to the three-dimensional MIKE SHE (Case 2-2) and MODFLOW (Case 2-4) codes, taken as references. In Case 2-3, the flexibility of BOUSS2D for handling complex geometries was demonstrated, through the simulation of a geological discontinuity embedded into a homogeneous aquifer.

The different analyses suggest that the BOUSS2D allows a significant flexibility as compared to the traditional groundwater flow models because of its ability to deal with unstructured and irregular meshes and thus with complex boundaries. In particular the coupling with a more realistic description of the river represented by polygon boundaries rather than by rectangular mesh cells is interesting in that context. Through the use of unstructured meshes, BOUSS2D needs less calculation nodes for the modeling and as such is less time consuming. Furthermore, as the continental surface heterogeneity is better represented through homogeneous modeling units, the specification of parameters can be facilitated, avoiding overparameterization problems.

The next step in the current research framework will be to include the BOUSS2D model into an integrated hydrological model. It will be coupled with other hydrological processes, such as unsaturated zone flow, evapotranspiration, and river flow, to derive a hydrological model, using both structured and unstructured mesh configurations, for handling appropriately natural heterogeneities (Dehotin and Braud 2008). Preliminary tests including the coupling with a module of water transfer within the unsaturated zone and real life tests cases were published by Dehotin (2007). However further testing is still required before being able to issue meaningful conclusions on the results of this coupling.

Acknowledgments

Special thanks go to the International Service of CEMAGREF for funding the stay of the second writer at CEMAGREF-Lyon.

Notation

The following symbols are used in the paper:

A_i = area of the mesh V_i (L^2) on horizontal plan;
d_{ik} = distance between X_i and X_k (L);
d_{ri} = distance between X_i and the interface e_{ik} along the vector $\boldsymbol{v_{ik}}$ (L);
e_{ik} = interface between V_i and V_k;
F_{ib} = center of the interface between V_i and the domain boundary;
F_{ik} = center of the interface between V_i and V_k;
h_b = imposed hydraulic head of at the domain boundary along V_i (L);
h_i = mean hydraulic head of V_i (L);
h_k = mean hydraulic head of V_k (L);
K_i = saturated hydraulic conductivity of the mesh V_i (LT^{-1});
L_{ik} = length of the exchange surface, between V_i and its adjacent meshes V_k (L);
M_i = projection of X_i on the perpendicular to the interface e_{ik}, through F_{ik};
M_k = projection of X_k on the perpendicular to the interface e_{ik}, through F_{ik};
$\boldsymbol{M_iM_k}$ = vector from M_i to M_k;
$\boldsymbol{m_k}$ = corresponds to the unit vector from X_k to M_k;
N_{vi} = number of neighbor meshes to V_i;
$\boldsymbol{n_{ik}}$ = perpendicular unit vector to the interface e_{ik} from X_i to X_k;
T_i = transmissivity of the mesh V_i (L^2T^{-1});
T_{ik} = transmissivity at the interface between V_i and V_k (L^2T^{-1});
T_k = transmissivity of the adjacent mesh V_k (L^2T^{-1});
$\boldsymbol{s_i}$ = unit vector from X_i to M_i;
$\boldsymbol{t_{ik}}$ = perpendicular unit vector to $[X_i,X_k]$;
$\boldsymbol{u_{ik}}$ = parallel unit vector to the interface $\boldsymbol{e_{ik}}$;
V_i = current mesh;
V_k = adjacent meshes to V_i;
$\boldsymbol{v_{ik}}$ = parallel unit vector to $[X_i,X_k]$;
X_i and X_k = centers of the meshes i and k;
α_i = ratio $F_{ik}X_k/F_{ik}X_i$;
Γ_i = contour of the mesh $V_i \cdot e_{ik} \in \Gamma_i$;
θ_{ik} = angle between $[X_i,X_k]$ and the perpendicular to the interface e_{ik}; and
$\|\boldsymbol{M_iM_k}\|$ = norm of the vector from M_i to M_k (L).

Subscripts

$_b$ = boundary segment of the mesh V_i;
$_i$ = current mesh V_i;
$_{ik}$ = interface between the meshes V_i and V_k; and
$_k$ = adjacent meshes V_k.

References

Aavatsmark, I. (2002). "An introduction to multipoint flux approximations for quadrilateral grids." *Computat. Geosci.*, 6(3), 405–432.

Aavatsmark, I., Barkve, T., Bøe, Ø., and Mannseth, T. (1994). "Discretisation on non-orthogonal, curvilinear grids for multiphase flow." *Proc., 4th European Conf. on the Mathematics of Oil Recovery*, Røros, Norway.

Abbott, M. B., Bathurst, J. C., Cunge, J. A., O'Connell, P. E., and Rasmussen, J. (1986a). "An introduction to the European Hydrological

System—Systeme Hydrologique Europeen, 'SHE', 1: History and philosophy of a physically-based, distributed modeling system." *J. Hydrol.*, 87, 45–59.

Abbott, M. B., Bathurst, J. C., Cunge, J. A., O'Connell, P. E., and Rasmussen, J. (1986b). "An introduction to the European Hydrological System—Systeme Hydrologique Europeen, 'SHE', 2: Structure of a physically-based, distributed modeling system." *J. Hydrol.*, 87, 61–77.

Anderson, M., and Woessner, W. W. (1992). *Applied groundwater modeling: Simulation of flow and advective transport*, Academic, San Diego.

Barth, T. (1994). "Aspects of unstructured grids and finite volume solvers for the Euler and Navier-Stockes equation." *Proc., VKI Lectures Series*, Van Kareman Institue, INIST-CNRS BELGIQUE.

Barth, T., and Ohlberger, M. (2004). "Finite volume methods: Foundation and analysis." *Encyclopedia of computational mechanics*, 57, John Wiley & Sons, Ltd.

Branger, F., Braud, I., Viallet, P., and Debionne, S. (2008). "Modeling the influence of landscape management practices on the hydrology of a small agricultural catchment." *Proc., 8th Int. Conf. on Hydro-Sciences and Engineering (ICHE-2008)*, ICHE, Japan.

Cai, Z. (1990). "On the finite volume element method." *Numerische Mathematik*, 58(1), 713–735.

Castany, G. (1966). *Prospection et exploitation des eaux souterraines*, Dunod, Paris.

Coudière, Y., Vila, J. P., and Villedieu, P. (1996). "Convergence of a finite volume scheme for a diffusion problem." *Finite volumes for complex applications: Problems and perspectives*, F. Benkhaldoun and R. Vilsmeier, eds., Hermes, Paris, 161–168.

de Marsily, G. (1981). *Quantitative hydrogeology: Groundwater hydrology for engineers*, Ed Masson, Paris.

Dehotin, J. (2007). "Prise en compte de l'hétérogénéité spatiale des surfaces continentales dans la modélisation hydrologique spatialisée. Application au Haut-bassin de la Saône." Ph.D. thesis, Université Joseph Fourier, Grenoble, France, ⟨http://cemadoc.cemagref.fr/exl-php/cadcgp.php?MODELE=vues/p_recherche_publication/home.html&VUES=p_recherche_publication⟩ (France).

Dehotin, J., and Braud, I. (2008). "Which spatial discretisation for distributed hydrological models? Proposition of a methodology and illustration for medium to large-scale catchments." *Hydrology Earth Syst. Sci.*, 12, 769–796.

Edwards, M. G. (2002). "Unstructured, control-volume distributed, full-tensor finite-volume schemes with flow based grids." *Comput. Geosci.*, 6(3–4), 433–452.

Edwards, M. G., and Rogers, C. (1994). "A flux continuous scheme for the full tensor pressure equation." *Proc., 4th European Conf. on the Mathematics of Oil Recovery*, Røros, Norway.

Edwards, M. G., and Rogers, C. (1998). "Finite volume discretization with imposed flux continuity for general tensor pressure equation." *Comput. Geosci.*, 2, 259–290.

Eymard, R., Gallouet, T., and Herbin, R. (1997). "Finite volumes method." *Handbook of numerical analysis*, P. Ciarlet and J. L. Lyons, eds., Vol. 7, 713–1020.

Eymard, R., Gutnic, M. l., and Hilhorst, D. (1999). "The finite volume method for Richards equation." *Comput. Geosci.*, 3(3/4), 259–294.

Ivanov, V. Y., Vivoni, E. R., Bras, R. L., and Entekhabi, D. (2004). "Catchment hydrologic response with a fully distributed triangulated irregular network model." *Water Resour. Res.*, 40(11), 23 p.

Jayantha, A. (2005). "A second order control-volume finite element least-squares strategy for simulating diffusion in strongly anisotropic media." *J. Comput. Math.*, 23, 1–16.

Jayantha, A., and Turner, I. (2001). "A comparison of gradient approximations for use in finite-volume computational models for two-dimensional diffusion equations." *Numer. Heat Transfer, Part B*, 40, 367–390.

Jayantha, A., and Turner, I. (2003a). "Generalised finite volume strategies for simulating transport in strongly orthotropic porous media." *ANZIAM J.*, 44, C443–C463.

Jayantha, A., and Turner, I. (2003b). "On the use of surface interpolation techniques in generalised finite volume strategies for simulating transport in highly anisotropic porous media." *J. Comput. Appl. Math.*, 152, 199–216.

Loudyi, D., Falconer, R. A., and Lin, B. (2007). "Mathematical development and verification of a non-orthogonal finite volume model for groundwater flow applications." *Adv. Water Resour.*, 30, 29–42.

McDonald, M. G., and Harbaugh, A. W. (1988). "A modular three-dimensional finite difference ground-water flow model." *U.S. Geology Survey techniques of water—Resources investigations, book 6*, Department of the Interior, Reston, Va.

Murthy, J. Y., and Mathur, S. R. (1998). "Computation of anisotropic conduction using unstructured meshes." *Numer. Heat Transfer, Part B*, 31, 195–215.

Pal, M., Edwards, M. G., and Lamb, A. L. (2006). "Convergence study of a family of flux-continuous, finite-volume schemes for the general tensor pressure equation." *Int. J. Numer. Methods Fluids*, 51(9–10), 1177–1203.

Schlumberger Water Services (SWS). (2007). *Visual MODFLOW premium demo tutorial*, Waterloo, Canada.

Siek, J. G., and Lumsdaine, A. (1998a). "The matrix template library: A generic programming approach to high performance numerical linear algebra." *Proc., ECOOP Workshops*, Springer (LNCS), Belgium.

Siek, J. G., and Lumsdaine, A. (1998b). "The matrix template library: A unifying framework for numerical linear algebra." *Proc., ECOOP Workshops*, Springer (LNCS), Belgium.

Siek, J. G., Lumsdaine, A., and Lee, L. Q. (1998). "Generic programming for high performance numerical linear algebra." *Proc., SIAM Workshop on Object Oriented Methods for Inter-operable Scientic and Engineering Computing (OO'98)*, SIAM Press, United States.

Theis, C. V. (1935). "The relation between the lowering of the piezometric surface and the rate and duration of discharge of a well using ground-water storage." *Trans., Am. Geophys. Union*, 16, 519–524.

Tison, L. J. (1953). "Theory of rivers in permanent movement, filtration phenomena." *Hydraul. Corses*, 2, 265–430.

Turkel, E. (1985). "Accuracy of schemes with nonuniform meshes for compressible fluid flows." *ICASE Rep.*, NASA, United States, Virginia, 43–85.

Turner, I. W., and Ferguson, W. J. (1995). "An unstructured mesh cell-centered control volume method for simulating heat and mass transfert in porous media: Application to soft wood drying, part I: The isotropic model." *Appl. Math. Model.*, 19, 654–667.

van der Vorst, H. A. (1992). "A fast and smoothly converging variant of bi-CGSTAB for the solution of nonsymmetric linear systems." *SIAM J. Sci. Stat. Comput.*, 13, 631–644.

Verma, S., and Aziz, K. (1997). "A control volume scheme for flexible grids in reservoir simulation, SPE 37999." *Proc., 14th SPE Reservoir Simulation, Symp.*, SPE, Dallas, Tex., 215–227.

Viallet, P., et al. (2006). "Towards multi-scale integrated hydrological models using the LIQUID framework." *Proc., 7th Int. Conf. on Hydroinformatics*, SHF, Nice, France, 542–549, ⟨http://www.hydrowide.com/liquid/⟩ (March 27, 2010).

Vivoni, E. R., Ivanov, V. Y., Bras, R. L., and Entekhabi, D. (2004). "Generation of triangulated irregular networks based on hydrologic similarity." *J. Hydrol. Eng.*, 9, 288–302.

J. Hydrol. Eng. 2011.16:108-125.